Development of efficient amplification method of DNA hydrogel and composite-type DNA hydrogel for photothermal immunotherapy

（DNA ハイドロゲルの効率的増幅法および光熱免疫療法のための複合材料型 DNA ハイドロゲルの開発に関する研究）

２０１５

矢田　智也

Preface

Deoxyribonucleic acid (DNA) is a biomolecule used to encode, transfer, decode and transcribe genetic information in living organisms on the earth. The molecule was firstly discovered by a Swiss physician Friedrich Miescher as "nuclein", DNA with associated proteins, from human pus cells in 1869[1]. The term of "nucleic acid" was introduced by Richard Altmann in 1889[2] when he succeeded to remove proteins from nuclein, and demonstrated that the deproteinized material was acidic material. In those early days, it was thought that the nucleic acid functioned in chromosomal stability and maintenance, and the proteins played the role of genetic material. However, three findings in the 1920s-1960s concluded that the nucleic acid, DNA, was the genetic material. In 1920s, Frederick Griffith showed that *Streptococcus pneumoniae* could transform into a different strain with "*transforming principle*"[3]. In 1944, Oswald T. Avery[4] presented experimental evidence showing that DNA had transforming ability. In 1952, Alfred Hershey and Martha Chase[5] confirmed that DNA is the genetic material by a series of "Hershey–Chase Experiment". In 1953, James Watson and Francis Crick[6] discovered the DNA double helix structure, and this discovery dramatically changed the focus of modern genetics, and opened the door of a new era in biology. In 2003, in 50 years of the great discovery, it was reported that the whole sequence of the human genome was completed at last[7]. The aspect of DNA as genetic material has been in the center of the biological research focus.

Many scientists have focused on other aspects of DNA than the genetic material, and made efforts to put DNA to practical use. From a chemical perspective, DNA is a polymer consisting of deoxyribose, phosphate, and four types of base including adenine (A), guanine (G), cytosine (C), and thymidine (T). DNA forms double helical structure through hydrogen bonds between A-T and G-C, whose diameter and helical rise in ordinary B-form DNA are about 2 nm and 0.34 nm/base, respectively[8]. The nature of the nucleic acids to form double-stranded structure with their complementary strand plays key roles in the central dogma of biology, including DNA polymerization, RNA transcription, interactions between mRNA and tRNA for translation in ribosome[9]. Recently, this ability to form double-stranded structure has been exploited to construct a variety of unnatural three dimensional nano-scale DNA structures. This new type of technology called "DNA nanotechnology" has attracted increasing attention[10]. In 1982, Nadrian C. Seeman and coworker pioneered DNA nanotechnology thorough the report that the branch-structured DNA could be created by synthesis of DNA with well-designed sequences[11]. A report by Paul W. K. Rothemund et al. in 2006[12] accelerated its attraction for applications in a number of fields. They prepared materials of arbitrary two-dimensional shapes, including a smiley face, by hybridizing a long

single-stranded DNA scaffold and multiple 'staple strands' to hold the scaffold in place, This method, known as "DNA origami", allows the arrangement of a large number of oligodeoxynucleotides (ODNs) with nano- to micro-meter precision, and made it possible to create highly complex and large structures. To date, DNA nanotechnology has been used in practical applications such as optical detection for microanalysis, diagnostics for pathogens, and drug delivery[13, 14, 15].

In innate immunity, nucleic acid is one of the molecules that trigger immune response[16]. For many years, it had been believed that innate immunity responds to pathogens in nonspecific manner, but the dogma was challenged by the discovery of Toll-like receptors (TLRs) as pattern recognition receptors (PRRs)[17, 18]. Extensive researches in this field have revealed that innate immunity responds to life crisis by recognizing specific molecules called pathogen-associated molecular patterns (PAMPs) and damage-associated molecular patterns (DAMPs)[19]. DNA is recognized by DNA sensors of TLR-9, DNA-dependent activator of IRFs (DAI), stimulator of interferon genes (STING) pathway as both PAMPs (exogenous DNA) and DAMPs (endogenous DNA)[20]. CpG DNA is a TLR-9 ligand that induces cytokine production from dendritic cells and macrophages through binding to TLR-9 in endosome after cellular internalization[21].

One of the hottest fields in nucleic acid researches is a trial to use nucleic acids as a new drug modality. Since nucleic acids are biomolecules which control a lot of biological and pathological mechanisms in nature, nucleic acid drug has been widely expected to be able to access targets more efficiently than other modalities do. However, due to still remaining big challenges in drug delivery, all types of nucleic acid drugs, including aptamer, decoy, antisense, small interfering RNA (siRNA), micro RNA (miRNA) and CpG DNA, have not shown their whole potential[22].

Social health and economy in the globalized world has greatly increased the value of vaccination. In recent years, researchers have expanded the scope of vaccines, and the target of vaccines is no longer limited to infectious diseases. Vaccines for a wide range of diseases including cancer, autoimmunity, allergy, and degenerative neurological diseases are under development[23, 24, 25]. To achieve successful vaccination for these diseases, it is required to induce immune responses against antigens from not infectious pathogens but self. There are, therefore, increased needs in development of immune adjuvant which enhances immune response strongly and safely[26].

In these situations, my department, Department of Biopharmaceutics and Drug Metabolism (the Department), has tried to develop a novel immune adjuvant by potentiating CpG ODN with DNA nanotechnology (Figure 1)[27]. In 2008, the Department discovered that it

was possible to potentiate the immunostimulatory activity of CpG DNA by forming three ODNs into a tripod-like structure, which was associated with enhanced cellular uptake by TLR9-positive cells[28, 29]. Subsequently, the Department showed that the potentiation by forming polypod-like structures was further expanded by increasing the number of pods from three to eight[30, 31]. The Department discovered that DNA dendrimer prepared through ligating polypod-like structured DNAs, or polypodnas, is able to stimulate efficiently immune cells to produce cytokines[32]. The Department also demonstrated that DNA hydrogel generated by enzymatically ligating polypodnas carrying adhesive ends with palindromic sequences is useful to co-deliver CpG DNA as an immunostimulatory agent and doxorubicin as an anti-cancer agent[33]. Moreover, the Department successfully developed and reported[34] a patented technology called "self-gelatinizable nucleic acid"[35] which enabled generation of DNA hydrogel through a self-assembling process by elongation of adhesive ends of nanostructured DNAs. The DNA hydrogel prepared by this technology has potential to become a quite unique, ideal, and novel vaccine adjuvant with following characteristics: (1) It is safe because it is composed of only DNA, not containing residual linking agents such as protein ligases and cross-linking chemical agents; (2) its properties can be designed by arranging the DNA sequences of adhesive ends and the structure of the building blocks; (3) the bioactivity is also designable by DNA sequence; (4) it is injectable and sprayable; (5) it forms hydrogel immediately at the administered site; (6) it is possible to sterile filtration and freeze-dry to prepare sterile products; (7) it is able to incorporate antigens or other bioactive materials; and (8) it is able to sustained-release materials incorporated.

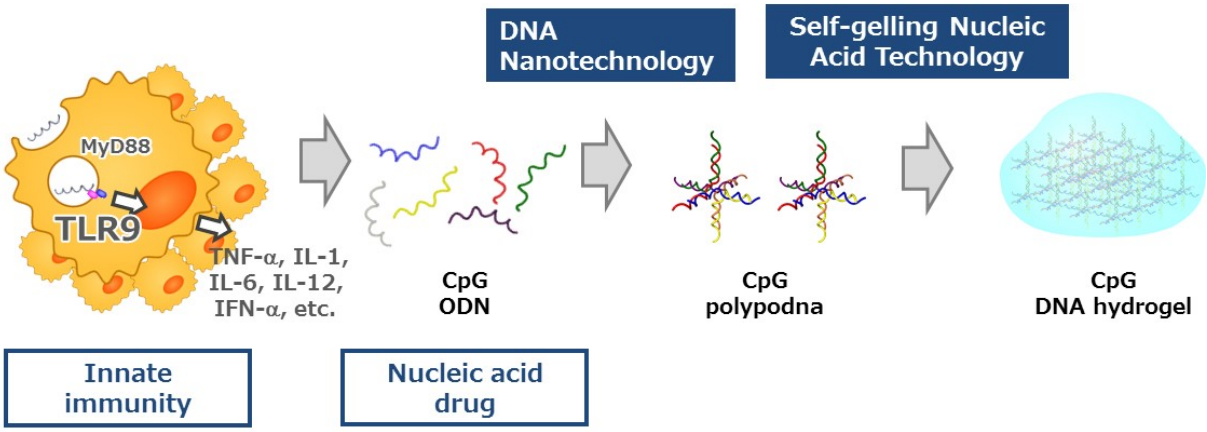

Figure 1：**Development of Polypodna Based DNA Hydrogel for Immunoadjuvant.**

To expand the future potential of the self-gelling DNA hydrogel for biomedical

applications, I have made a series of studies (Figure 2). Synthesis cost is one of the biggest challenges from the viewpoint of practical application. To provide its solution, I have made an attempt to develop a novel amplification method of self-gelling polypodna, which was presented in Chapter 1. Next, I tried to synthesize a novel composite-type hydrogel for photothermal immunotherapy by using the self-gelling nucleic acid technology, and evaluated its efficacy in tumor-bearing mice in Chapter 2. Here, I report these studies.

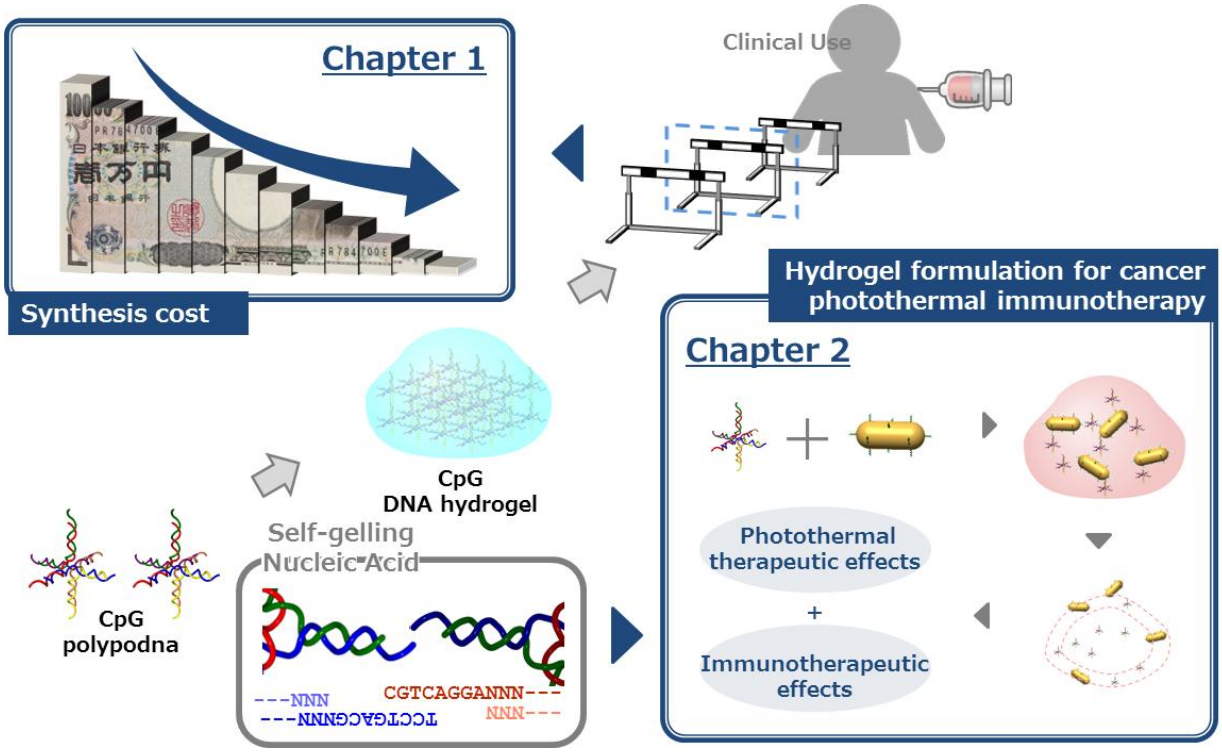

Figure 2： Scopes of this Doctoral Thesis.

Contents

Chapter 1 : Efficient Amplification of Self-gelling Polypod-like Structured DNA by Rolling Circle Amplification and Enzymatic Digestion

1.1 Introduction

Synthesis cost is one of the major limiting factors for practical use of biomaterial composed of nanostructured DNAs such as polypodna-based self-gelling DNA hydrogel in macroscale to biomedical area[36, 37]. Nanostructured DNAs are typically made of chemically synthesized long single-stranded ODNs (30-100 nt). Although synthesis technologies of single-stranded ODNs have progressed tremendously to reduce the synthesis cost since the first report on solid-phase synthesis method in 1960s[38], the accuracy and efficiency have not reached the levels in nature[39]. In the artificial synthesis, the coupling efficiency never reaches 100% at each step because of chemical and physical restraints. Synthesis cost increases as increasing the length of nucleotides, because the yield generally decreases in an exponential manner[40]. Enzymatic synthesis can be an attractive alternative for chemical synthesis because enzymes quickly copy and amplify any template sequence with low error rates compared with chemical processes. Phi29 DNA polymerase, obtained from *Bacillus subtilis* phage *phi29*, possesses the functions not only for quick generation of polynucleotides, but also for strand displacement and proofreading under isothermal conditions[41, 42, 43]. Rolling circle amplification (RCA) using this enzyme is able to produce long single strands of the tandem-repeating sequence, which is complementary to the circularized single-stranded DNA template[44].

There have been some successful reports of Phi29 DNA polymerase-based amplification of simple DNA, such as linear oligodeoxynucleotide and DNA aptamer[45, 46, 47, 48], or semi-large scale amplification of complicated DNA structures[49]. However, no attempts have been made on the amplification of functional structured DNA such as self-gelling building blocks that spontaneously form DNA hydrogel under proper conditions. Here, I propose a highly efficient production technique for self-gelling polypodna by using RCA-based amplification, and demonstrate its feasibility through the amplification of two types of self-gelling nanostructured DNAs.

1.2 Methods

[1] Preparation of Template ODNs

All oligodeoxynucleotides were purchased from Integrated DNA Technologies, Inc (Coralville, IA, USA). The sequences of the oligodeoxynucleotides used are summarized in Table 1. A linear 5′ -phosphorylated template oligodeoxynucleotide, template ODN (50 μM), was self-annealed by heating at 95°C for 2 min, 75°C for 3 min, then gradually cooled down to 4°C. The annealed oligodeoxynucleotide was ligated at 16°C for 16 h in solution containing 10 U/μL T4 DNA ligase (Takara Bio, Otsu, Japan), 66 mM Tris-HCl (pH 7.6), 6.6 mM $MgCl_2$, 10 mM dithiothreitol (DTT), and 0.1 mM ATP. Non-circularized linear oligonucleotides were removed by reaction with 25 U/mL exonuclease I (Takara Bio, Shiga, Japan) and 1000 U/mL exonuclease III (Takara Bio) at 37°C for 30 min.

[2] RCA-based Amplification of Polypodna Precursors

An RCA primer was designed to hybridize to the single stranded sequence of the circularized template. Equivalent amounts of the circularized template and the primer were mixed together, and these were annealed by heating at 95°C for 2 min, 75°C for 3 min, then gradually cooled down to 4°C. The resultant mixture (10 μM) was amplified by incubating at 30°C for 16 h in a solution containing 2.5 U/μL Phi29 DNA polymerase (New England Biolabs, Ipswich, MA, USA), 50 mM Tris-HCl (pH 7.5), 10 mM $MgCl_2$, 10 mM $(NH_4)_2SO_4$, 4 mM DTT, 200 μg/ml BSA, and 2.5 mM dNTP (Invitrogen, Carlsbad, CA, USA)

[3] Polypodna Production by Restriction Digestion

The highly viscous RCA product was incubated in 2 mM EDTA (Sigma-Aldrich, St. Louis, MO, USA) at 80°C for 15 min to solubilize the product. After purification by size-exclusion chromatography, the resultant large molecular weight DNA was digested with 0.1 U/μL TspRI (New England Biolabs) in solution containing 50 mM potassium acetate, 20 mM Tris-acetate, 10 mM magnesium acetate, and 100 μg/ml BSA. The product was purified by size-exclusion chromatography to remove low molecular weight DNA waste. Restriction digestion with TspRI was performed at 50°C, which was determined to be the optimal temperature for digestion with TspRI, based on preliminary experiments.

[4] Polypodna Formation

The RCA product obtained after restriction digestion was annealed as reported previously[34]. Briefly, the 1.5- or 2 mM-DNA products for tripodna or tetrapodna, respectively, were heated

to 95°C and cooled gradually to 4°C. The formation of hydrogels was observed optically using blue dextran solution as previously reported[34].

[5] Oligodeoxynucleotide Analysis

DNA products in each step were analyzed by chip analysis using a MCE-202 MultiNA microchip electrophoresis system (Shimadzu Corporation, Kyoto, Japan) or by polyacrylamide electrophoresis (PAGE). Denaturing PAGE was carried out with 12% Acrylamide gel/ 7M Urea under 150 V for 60 min.

[6] Observation of RCA Product under Fluorescent Microscope

The appearance of the RCA product before and after EDTA treatment was observed under a fluorescent microscope (Biozero BZ-8000, KEYENCE, Osaka, Japan) after staining with SYBR-Gold (Molecular Probes, Eugene, OR, USA).

[7] Scanning Electron Microscope Imaging

The RCA product obtained after restriction digest was annealed under the above conditions. The structure of the annealed RCA products was then observed using a scanning electron microscope (TM3000, Hitachi, Tokyo, Japan) as reported previously[34].

[8] Atomic Force Microscope Imaging

Atomic force microscope images were obtained with a high-speed AFM system (Nano Live Vision, RIBM, Tsukuba, Japan) using a silicon nitride cantilever (BL-AC10EGS; Olympus, Tokyo, Japan)[50]. Briefly, the sample was adsorbed on a freshly cleaved mica plate pretreated with 0.1% aqueous 3-aminopropyltriethoxysilane for 5 min at room temperature and then washed three times with a buffer solution containing 20 mM Tris and 10 mM $MgCl_2$. To observe the elongation of the RCA products, aliquots were sampled at 0 (before initiation of the reaction), 1, and 4 h after the onset of the RCA reaction. Then, the collected samples were heated to 95°C to halt the reaction, annealed, and diluted to a DNA concentration of 30 nM to avoid hydrogel formation. Then, the samples were observed by AFM as described above.

Table 1 : Sequences of Oligonucleotides used in Chapter 1

ODN	Sequence (5′→3′)
Tripodna	
Template 1	tgc gcc aat ggc aaa agc caa tgg cgc acg tcg tag tgc att gac agc gtc tag cta gcc aat ggc aaa agc caa tgg cta gct aga cgc tgt caa gca gac gtc gat caa gcc aat ggc aaa aaa aaa aaa aaa aaa aaa aaa aaa aaa aaa aaa aaa aaa gcc aat ggc ttg atc gac gtc tgc tat gca cta cga cg
Primer 1	ttt ttt ttt ttt ttt ttt ttt ttt t
Tetrapodna	
Template 2-1	cta gac cgt gtc atg acg ctc agc tgc aag cca ctg gct tcg aaa aaa aac gaa gcc ag
Template 2-2	tgg ctt gca gct gag cgt caa gca gac gtc gat caa gcc agt ggc ttg
Primer 2	cgt cta gca agc cac tgg ct
Template 3-1	atc gac gtc tgc tgc acg tcg tag tgc aag cca gtg gct tcg aaa aaa aac gaa gcc ac
Template 3-2	tgg ctt gca cta cga cgt gct gac agc gtc tag caa gcc act ggc ttg
Primer 3	agc aga cgt cga tca agc cag tgg ct

1.3 Results

1.3.1 Schematic Amplification Method for Self-gelling Tripodnas

Figure 3 illustrates the scheme of the RCA-based mass amplification of simple structured tripodnas with adhesive 5′-ends.

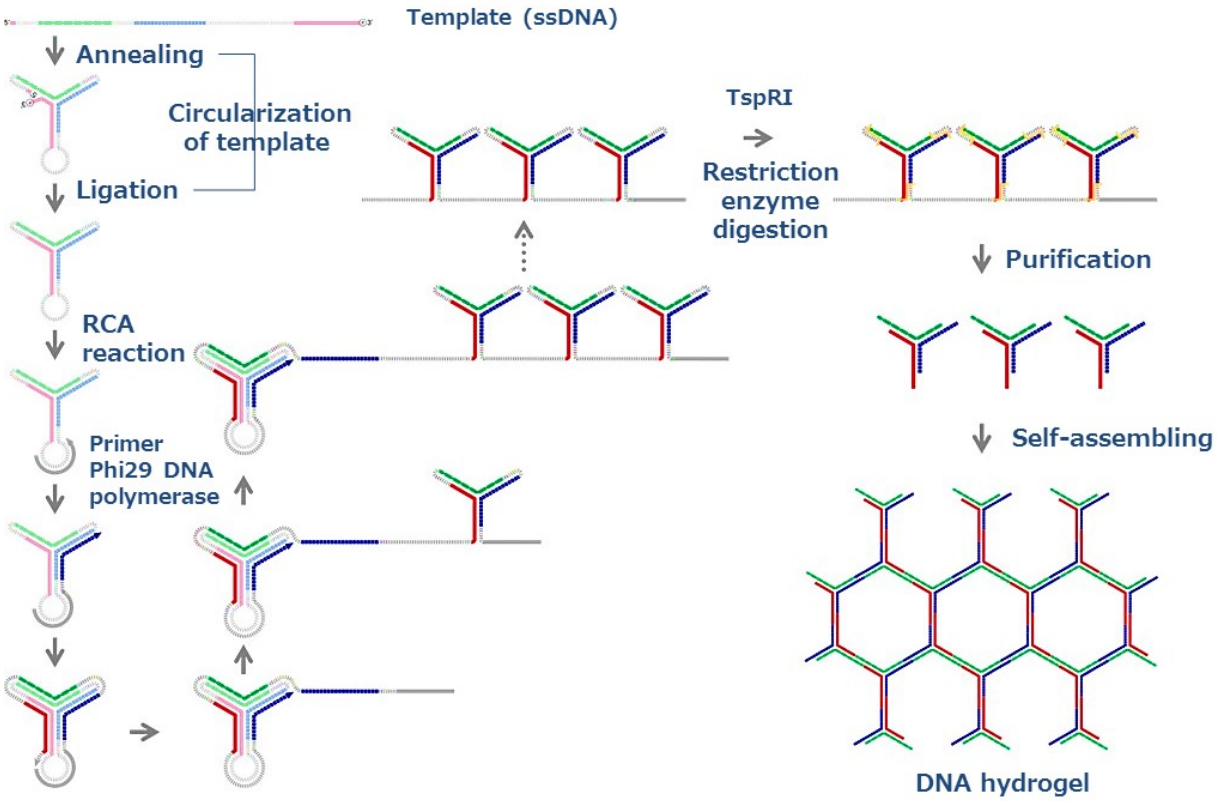

Figure 3: Schematic Diagram of the Mass Amplification of Simple Structured Self-gelling Tripodnas. The template oligodeoxynucleotides are designed to satisfy the following requirements: (a) the tripodna automatically forms by self-assembly; (b) each pod of the tripodna contains a 9 base long TspRI restriction digest site; (c) Each 5′-terminal end is phosphorylated in order to ligate with 3′-terminal within the tripodna body, (d) connecting chain is added to the 3′-terminal of the tripodna to allow tripodna to be connected to one another. The designed templates are amplified via the following steps: (1) The template ssODNs are circularized using T4 DNA ligase; (2) After annealing the primer (primer 1), the DNA template is amplified through rolling circle amplification technique using Phi29 polymerase; (3) Before enzyme digestion, the RCA product is treated with EDTA and folded; (4) Long single-stranded DNAs are digested using restriction enzyme; (5) The target sequences are purified by size chromatography; (6) The resultant DNAs self-assembled after annealing to form a hydrogel.

1.3.2 Demonstration Study for Amplification of Self-gelling Tripodna

<Circularization of Template DNA>

To amplify self-gelling tripodna, at first, a template single stranded DNA was circularized using T4-ligase. Figure 4 shows the microchip electrophoresis of the template before and after ligation using T4-ligase. There was no significant difference in the electrophoretic mobility of the template before and after ligation (Figure 4, lanes 1, 2). This could be because the template would be folded in a similar structure to the ligated, circularized one. To confirm the ligation, the non-ligated and ligated templates were digested by exonuclease I/III (Figure 4, lanes 3, 4). Only the ligated template was resistant to the digestion (Figure 4, lane 4), indicating that the template was circularized by T4-ligase. To proceed DNA elongation, the non-circularized template oligonucleotides were removed by exonuclease digestion.

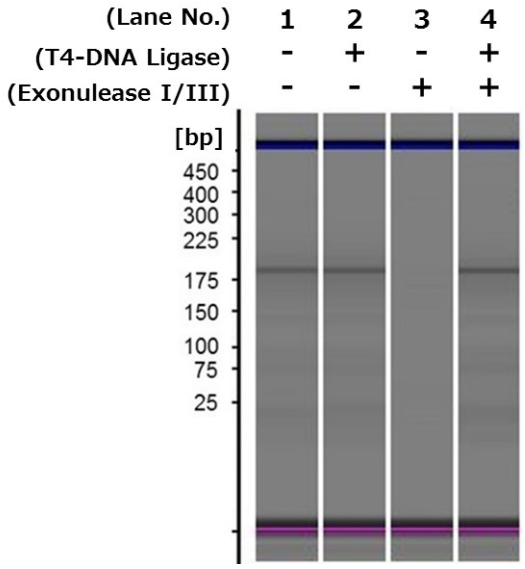

Figure 4: Chip Analysis of Template DNA Circularization. Lane 1, non-ligated template; lane 2, ligated template; lane 3, non-ligated template digested by exonuclease I/III; lane 4, ligated template digested by exonuclease I/III.

<DNA Elongation by RCA>

The circularized template was replicated by RCA, whose reaction was monitored by AFM imaging. The Y-shaped mono-structured templates were observed at the initial of reaction (Figure 5 (a)), and the ODN chain was elongated with time (Figure 5 (b-c)). A long reaction time resulted in highly viscous products as shown in Figure 5 (d). Agarose gel electrophoresis showed that the electrophoresis mobility of the RCA product was much lower than 10 kbp

band, indicating that the DNA was successfully elongated by RCA (Figure 5 (e), lane 2).

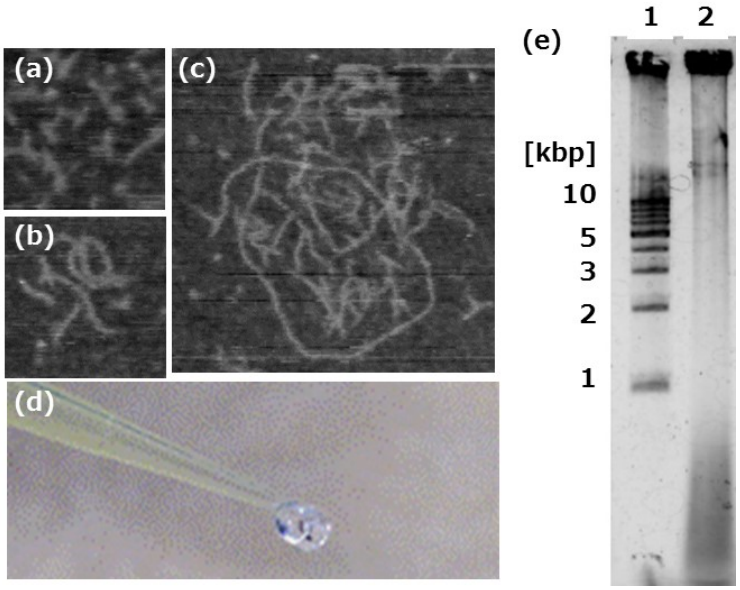

Figure 5: DNA Elongation by RCA. (a) 0 h (before initiation of the RCA reaction), (b) 1 h, (c) 4 h. (d) RCA product after 16-h reaction. (e) Agarose gel analysis of RCA product. Lane 1, 1-kbp ladder; lane 2, RCA product.

<Analysis of RCA Product and Restriction Enzyme Digestion>

Then, the RCA product was purified by phenol-chloroform extraction and ethanol precipitation protocols. After removing ethanol, the DNA was digested with TspRI and the digested sample was analyzed by denaturing PAGE (Figure 6 (a)). A strong band with quite low electrophoresis mobility and little weak bands with high mobility were observed, indicating that the digestion generated only a small amount of short ODN products (Figure 6 (a) lane 3). To understand the cause of this unsuccessful digestion, the structure of the RCA product was visualized under a fluorescent microscope. Staining the RCA product with SYBR Gold revealed that the RCA product contained many microparticles (Figure 6 (b)). Observation under a SEM showed that the microparticles were in microflower-like structures (Figure 6 (c)). It has been reported that RCA products are densely packed and resistant to enzyme digestion[51, 52]. Breaking down the microflower-like structure of the RCA product would be useful for the efficiency of its restriction digestion. Extensive studies on the microstructure of interfering RNAs, (RNAi)-microsponges produced by T7-RNA polymerase, have shown that the RNA microstructure was composed of magnesium pyrophosphate, and it was capable of being denatured by EDTA[53]. Pyrophosphate is a side product of the nucleotide coupling reaction, and it is produced in RCA. Therefore, it was assumed that the DNA microflower-like structure

generated by the RCA reaction is also composed of magnesium pyrophosphate, and is able to be denatured by EDTA. As expected, the microparticles in the RCA reaction solution were broken up by the addition of EDTA, followed by heating at 80°C for 15 min (Figure 6 (d)). After purification of polynucleotides by size-exclusion chromatography, the solution was heated to 95°C and cooled gradually down to 4°C to form tripodna into the long chain polynucleotides for restriction enzyme digestion. In this case, the polynucleotides were efficiently digested into short fragments. Denaturing PAGE analysis clearly showed that oligonucleotides were efficiently produced by restriction digestion of the RCA products after EDTA treatment (Figure 6 (a), lane 4).

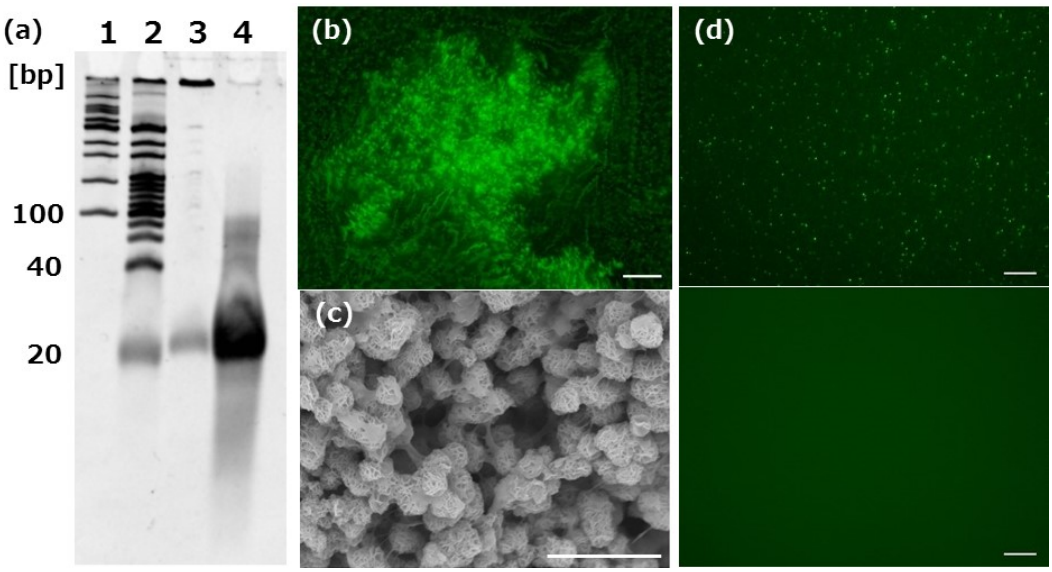

Figure 6: Analysis of RCA Product and Restriction Enzyme Digestion. (a) Denaturing PAGE analysis of RCA products before and after digestion by restriction enzyme. Lane 1, 100 bp marker; lane 2, 20 bp marker; lane 3, digested DNA fragments without EDTA treatment; lane 4, digested DNA fragments after EDTA treatment. (b) Fluorescent microscope image of the RCA product. The highly viscous RCA product was stained using SYBR Gold. Scale bar = 100 µm. (c) SEM image of the RCA product. RCA product was dehydrated using ethanol, and freeze-dried. Particle size of microflower-like structure was estimated around 2–3 µm, and similar to the structure of RNAi-microsponges previously reported[53]. Scale bar = 10 µm. (d) Fluorescent microscope image of RCA product before/after treatment of EDTA. (upper) Before EDTA treatment, microparticles were observed. (lower) After EDTA treatment, microparticles disappeared. Scale bar = 50 µm.

<Tripodna Based DNA Hydrogel Formation>

The oligonucleotides were purified by size-exclusion chromatography and were concentrated into 1.5 mM in saline through ethanol precipitation protocol. When annealed at 95°C, the products were not capable of being mixed with a solution containing blue dextran (Sigma-Aldrich, St. Louis, MO, USA) Figure 7 (a)), which suggested the formation of a hydrogel with micro network inner structure. To confirm the self-assembling of tripodnas, AFM imaging was performed in 30 fold diluted conditions. It showed that the products self-assembled into oligomers or multimers under the diluted conditions (Figure 7 (b)). Next, to assure the inner structure of generated DNA hydrogel, SEM observation was performed. Figure 7 (c) showed that the inner structure of the hydrogel obtained by this technique was comparable to that of the DNA hydrogel made up of tripodna with chemically synthesized oligodeoxynucleotides reported previously[35]. These results suggest that the DNA hydrogel is formed by self-assembly of the tripodnas through the sticky ends.

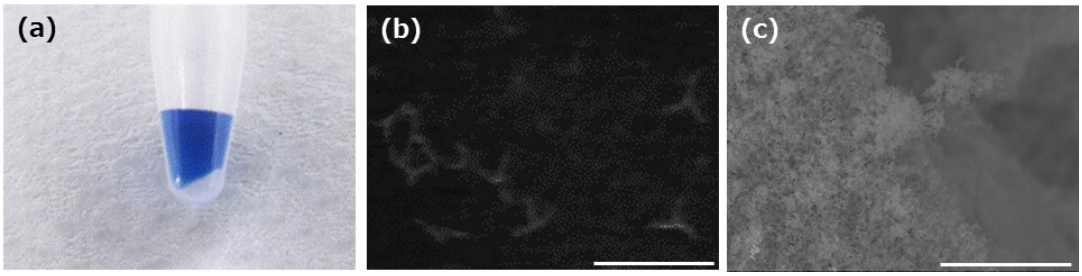

Figure 7 : Tripodna Based DNA Hydrogel Formation. (a) Optical image of resulting DNA hydrogel. The solution containing blue dextran (Sigma Aldrich, St. Louis, MO, USA) was added to check the hydrogel formation. Blue dextran did not instantly diffuse into hydrogel. (b) AFM image of the RCA product obtained using the tripodna template. Scale bar = 50 nm. (c) SEM image of resulting DNA hydrogel. Scale bar = 30 μm.

1.3.3 Schematic Amplification Method for Self-gelling Tetrapodna

Figure 8 illustrates the scheme of the RCA-based mass amplification of complex structured tetrapodnas with adhesive 5′-ends. To expand the method to apply for amplification of further complex nanostructured DNAs, a different scheme was designed. The template of complex structured DNAs are longer than that of simple ones since a complex structured DNAs require more nucleotides compared to simple ones. To avoid the costliness and technical difficulty associated with the preparation of a long template, a long template sequence is separated into multiple short sequences. The multiple templates are used for the RCA-based amplification and amplified through rolling circle amplification, separately.

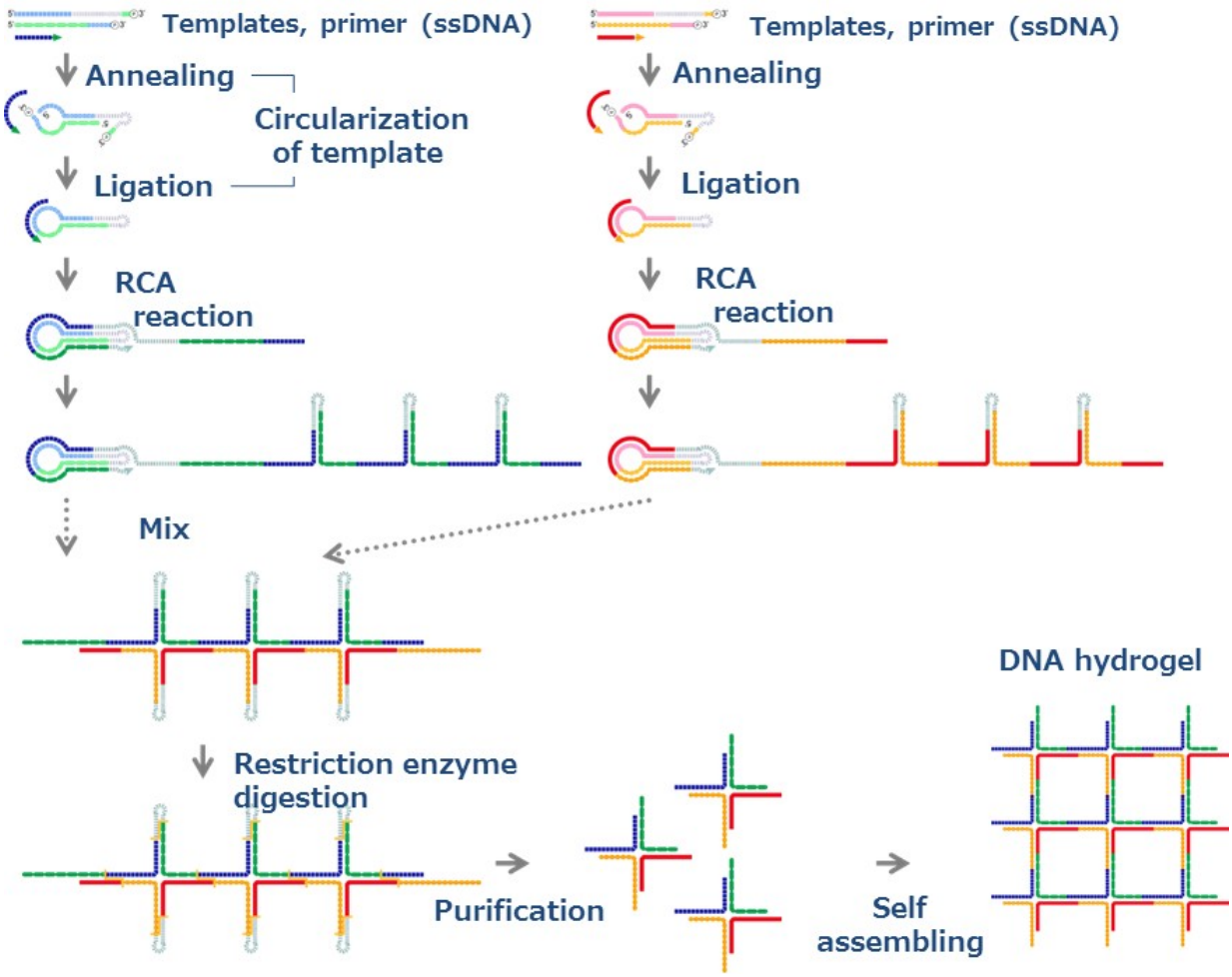

Figure 8 : Schematic Diagram of the Mass Amplification of Complicated Structured Self-gelling Tetrapodnas. Multiple short fragment templates are used to reduce cost, and different circular templates are constructed using these fragment templates and primers, separately. Except for these, the same protocol as described in Section 1.3.1 is used to amplify the templates.

1.3.4 Demonstration Study for Amplification of Self-gelling Tetrapodna

<Circularization of Template DNA and DNA Elongation by RCA>

Circularization of template DNA and DNA elongation reaction by RCA were performed in the same manners as a tripodna case except for the point that multiple template DNAs were used. Each template DNA also produced from two separate fragments. Figure 9 shows the microchip electrophoresis analysis of products at each step. The templates were ligated using T4-ligase, followed by digestion using exonuclease I/III. Figure 9 shows that the bands remained after the exonuclease digestion, and there was no significant difference in the electrophoretic mobility of the template before and after ligation, which was in the same manner as the case of tripodna amplification ((a) (b) lane 1, 2). Both templates were successfully replicated by RCA. (Figure 9, (a) (b) lane 3).

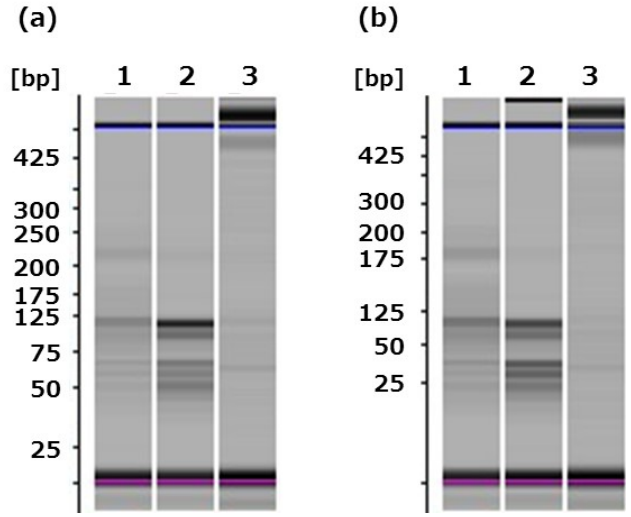

Figure 9 : Chip Analysis of Template DNA Circularization and DNA Elongation by RCA. RCA was performed separately from two small template DNAs (template-2, template-3) to amplify self-gelling tetrapodna. (a) Chip analysis for reactions from template-2. Lane 1, non-ligated template; lane 2, ligated template digested by exonuclease I/III. (b) Chip analysis for reactions from the template-3. Lane 1, non-ligated template; lane 2, ligated template digested by exonuclease I/III.

<Restriction Enzyme Digestion>

The RCA products were digested using TspRI, but it failed in same manner as the tripodna case. After EDTA treatment, the digestion succeeded to produce approximately 60 base fragments (Figure 10).

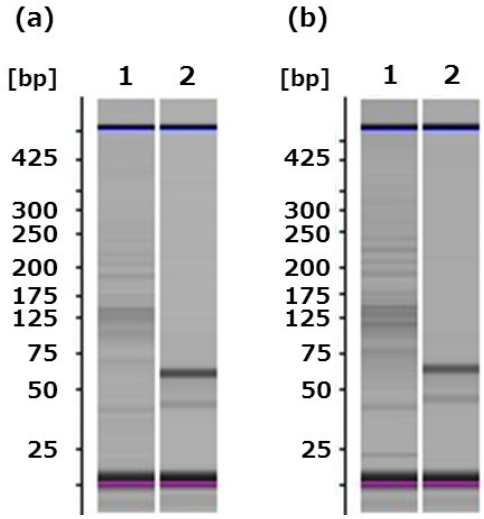

Figure 10 : **Chip Analysis of Restriction Enzyme Digestion.** (a) Microchip analysis of RCA products from template-2 before and after digestion by restriction enzyme. Lane 1, digested DNA fragments without EDTA treatment; lane 2, digested DNA fragments after EDTA treatment. (b) Microchip analysis of RCA products from template-3 before and after digestion by restriction enzyme. Lane 1, digested DNA fragments without EDTA treatment; lane 2, digested DNA fragments after EDTA treatment.

<Tetrapodna Based DNA Hydrogel Formation>

After the purification and annealing process, a hydrogel was formed (Figure 11(a)). The hydrogel was analyzed further in the same manner as tripodna case. Oligomers and multimers of tetrapodna units were observed under AFM imaging in dilute solutions (Figure 11 (b)). The inner structure of the hydrogel was similar to that of a tetrapodna-based hydrogel consisting of chemically synthesized ODNs (Figure 11 (c)).

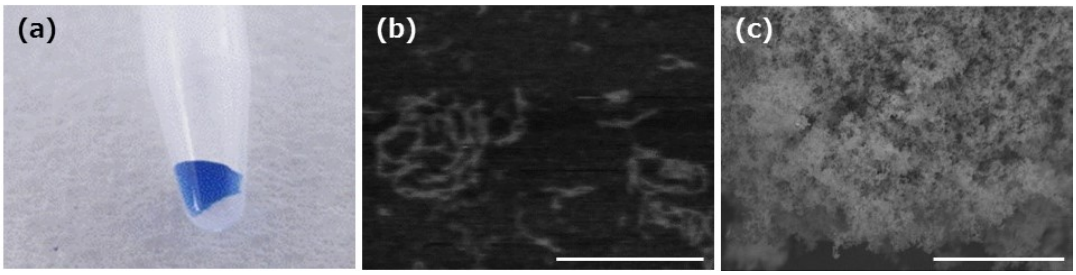

Figure 11 : **Tetrapodna Based DNA Hydrogel Formation** Optical image of the resulting DNA hydrogel. The solution containing blue dextran (Sigma Aldrich, St. Louis, MO, USA) was added to check the hydrogel formation. (b) AFM image of the RCA product obtained using the tetrapodna templates. (c) SEM image of resulting DNA hydrogel.

1.4 Discussion

This study demonstrated that tripodna and tetrapodna can be efficiently replicated in large quantities (approximately 300-fold) by RCA. This technique requires basic biochemical laboratory equipment and basic reagents, and can be performed with little technical difficulty. Although the DNA nanostructures covered in this study were relatively simple ones, i.e., tripodna and tetrapodna, as I proposed and demonstrated here, this technique can be expanded, and applied to complex DNA nanostructures. These include hexapodna, truncated octahedrons[54], octahedrons[55], tetrahedrons[56], and DNA buckyballs[57]. The results of the tetrapodna directly showed that the use of two or more templates can increase the complexity of DNA nanostructures without additional difficulties in both design and production.

Since this was a proof-of-concept study, the scale of the final products was in microgram scale, and there are still challenges to scale up the reaction volume for practical application. However, it is considered that the technique is useful to provide an alternative method to chemical synthesis for efficient amplification of such complex structured DNA building blocks as polypodna for expanding the application of DNA hydrogel. The overall costs for the preparation of tripodna and tetrapodna were less than those required for the ODNs for tripodna and tetrapodna, even under the conditions used for the small-scale study, although a strict comparison between them is difficult because of the large difference in the price for ODNs. Because the cost for phi29 DNA polymerase accounted for a significant proportion (more than 70%) of the total cost for the RCA-based amplification method of the present study, optimization of the RCA reaction would greatly reduce the total cost of this method.

Other restriction enzymes than TspRI can also be used to produce self-gelling polypodna. The principle underlying this approach can be easily applied to replicate other designs of polypodna and many other complex DNA nanostructures. There have been some reports that apply the RCA technique to the amplification of DNA nanostructures[45, 46, 47, 48, 49], but none of them mentioned unsuccessful enzyme digestion of the RCA products or the high viscosity of the RCA reaction solution. It might be because previous studies were conducted with low concentrations of DNA. In this study, rolling circle amplification was performed with a high DNA concentration to produce short ODN products for DNA nanostructures efficiently. The present study indicates for the first time that the degradation of the byproduct in the RCA reaction using EDTA enables us to increase the DNA concentration for RCA reaction. Therefore, the scheme that I describe here can provide a solution to overcome the major obstacle for large-scale production of DNA nanostructures.

In conclusion, I successfully developed an efficient synthesis method for self-gelling

polypod-like structured DNA that spontaneously forms DNA hydrogel under proper conditions. The results of this study will provide a new approach to amplify DNA nanostructures, and helps in expanding their practical applications.

Chapter 2 : Development of Composite-type DNA Hydrogel for Photothermal Immunotherapy

Chapter 2-1 : Development of Prototype Formulation and its Evaluation *In Vitro*

2.1 Introduction

Photothermal immunotherapy is a promising modality for cancer that combines local photothermal therapy and systemic immunostimulation[58, 59]. Photothermal therapy is a therapeutic strategy based on the localized photothermal stresses induced by penetrating near-infrared (NIR) laser and photosensitizing nanomaterials. Decades ago, it was considered that the purpose of photothermal therapy was simply to kill tumor cells, like surgical excision, by ablating to provide sufficient heat stress to induce cell necrosis[60]. It was believed that the higher temperature brought better therapeutic effects. However, increased evidence has revealed that heating tumors to the moderate temperature of 40-45 °C had a lot of therapeutic benefits including not only cell death but also immune stimulation[61]. Heat stress in the range of 40–45 °C is able to arrest cell proliferation and induce cell death[62]. When cells are exposed to heat stress, cells undergo several changes at molecular levels[63]. Elevated temperature affects cell membrane to lead changes in cell morphology, membrane potential, membrane fluidity and stability[64]. Heat-induced protein denaturation impacts a lot of cellular signaling and functions. Although nucleic acids are not damaged at 40-45 °C, enzymatic polymerization, repair and degradation processes are sensitive to the temperature, which greatly contributes to heat-induced cell-cycle arrest and cell death. In addition to these effects, tumor cells which suffered heat stress enhances the expression and release of heat shock proteins (HSPs) known as heat stress inducible proteins. Hsp70 is a member of the HSPs with a molecular mass of 70,000, playing roles as a chaperon within cells. Extracellular Hsp70 regulates diverse immune functions against tumor. Hsp70 released from heat stressed cells is able to directly bind to CD40, TLR2 and TLR4 on antigen presenting cells (APCs) to induce cytokine production and antigen uptake by the APCs[65, 66, 67, 68]. Moreover, Hsp70 is recognized by natural killer cells (NK cells) to enhance proliferation and activation of cell lysis activity[69, 70, 71, 72]. Hsp70, a chaperon, is able to bind tumor associated antigens (TAAs) through its polypeptide binding domain locating at C-terminal. The Hsp70-TAA complex is recognized by HSP receptors such as LOX-1 and CD91 on dendritic cells, macrophages and other APCs[65, 68],

and promotes the cross presentation of TAA to $CD8^+$ T cells via MHC class I to lead to tumor specific $CD8^+$ T cell responses[73, 74, 75].

To boost up these immune activities following photothermal therapy more efficiently and strongly, several types of immune adjuvants bearing photothermal activity have been investigated[76, 77, 78, 79, 80, 81, 82]. To my best knowledge, all these formulations are solution formulations, but from the viewpoint of targeted delivery, a hydrogel formulation would be more preferable. It was reported that DNA hydrogels prepared through "self-gelling nucleic acid" technology were promising for immunotherapy application because they were injectable, biodegradable, and highly immune active. Here, to obtain a photothermally active DNA based hydrogel formulation, a composite-type hydrogel was designed by applying the "self-gelling nucleic acid" technology between photosensitizer and polypodna. Gold nanoparticles (AuNPs), showing surface plasmon resonance with high extinction coefficient, have been widely used for application for photothermal therapy and drug delivery. Since the first report by Chad A. Mirkin et al. on spherical DNA assemblies composed of DNA and AuNPs [83], AuNPs have been applied for the delivery of small interfering RNA, antisense oligonucleotides, and CpG DNA as AuNP-ODN conjugates (AuNP-ODN)[84, 85, 86]. In addition, fortunately, ODNs on AuNPs contributes to stabilize the AuNPs, preventing them from forming agglomeration through electrostatic repulsion. In this chapter, AuNP-ODN and hexapodna were hybridized to prepare a novel composite-type hydrogel, and its therapeutic application was examined *in vitro*.

2.2 Methods

[1] Preparation of AuNP-DNA Nanocomposites

AuNPs with an average diameter of 50 nm were purchased from Sigma-Aldrich (St. Louis, MO, USA). All ODNs were purchased from Integrated DNA Technologies, Inc. (Coralville, IA, USA). The sequences of the ODNs used are summarized in Table 2. To prepare ODN-modified AuNPs, i.e., AuNP-ODN(cg)-A and AuNP-ODN(gc)-A, ODN(cg)-A or ODN(gc)-A, a CpG or GpC ODN with polyadenine sequence, was adsorbed onto the surface of AuNPs, respectively, according to the method previously reported by Juewen Liu et al[87]. Briefly, 500 mM citrate·HCl buffer (pH 3) was added to the mixture of AuNP and ODN to the final concentration of 10 mM, and the mixture was allowed to incubate at room temperature for 3 min. Then, the pH of the mixture was adjusted back to neutral by adding 500 mM HEPES buffer (pH 7.6), and was allowed to incubate for another 10 min at room temperature. The AuNP-ODNs were collected by centrifugation at 20,000×g, and washed with purified water. Separately, four types of hexapodnas, i.e., hPODNA(cg)-A, hPODNA(gc)-A, hPODNA(cg)-B, and hPODNA(gc)-B, were prepared by mixing equimolar six ODNs for each preparation as previously reported. Here

hPODNA(cg)-B and hPODNA(gc)-B contain the 8-nucleotide-long single-stranded 5′-ends complementary to the 5′-end of ODN(cg)-A and ODN(gc)-A, and the 8-nucleotide-long single-stranded 5′-ends of hPODNA(cg)-B and hPODNA(gc)-B are non-complementary to(and the same sequence as) ODN(cg)-A and OCN(gc)-A. Again, (cg) and (gc) indicate that the hexapodnas contain CpG or GpC sequence, respectively. The formation of these hexapodnas was assessed by PAGE analysis as previously reported[30]. Then, the following six types of samples were prepared by mixing equivolumes of two components at room temperature: (1) AuNP-hydrogel(cg), (2) AuNP-hydrogel(gc), (3) AuNP-ODN/hPODNA(cg), (4) AuNP-ODN/hPODNA(gc), (5) hydrogel(cg), and (6) hydrogel(gc). The combinations of the components used for each sample are summarized in Table 3. AuNP-hydrogel(cg), AuNP-hydrogel(gc), hydrogel(cg), and hydrogel(gc) are the formulations that are intended to form hydrogels, whereas AuNP-ODN/hPODNA(cg) and AuNP-ODN/hPODNA(gc) are the mixtures of AuNP-ODN and hexapodna, which will not form hydrogel.

[2] Scanning Electron Microscope Imaging

The structure of the AuNP-hydrogel(cg) was observed by scanning electron microscopy as reported previously[33]. Briefly, the AuNP-hydrogel(cg) was fixed with 2% glutaraldehyde at room temperature overnight, dehydrated with increasing concentrations of ethanol which was replaced with butyl alcohol, and freeze-dried. The dried material was observed using a field-emission scanning electron microscope (TM3000, Hitachi, Tokyo, Japan).

[3] Ultraviolet-Visible Absorption Spectra

Ultraviolet (UV)-visible absorption spectra were measured on NanoDrop 2000 spectrophotometer (Thermo Scientific, MA, USA) at a sample volume of 1 μL.

[4] Evaluation of Photothermal Behavior

The AuNP-hydrogel(cg) was exposed to continuous wave laser irradiation at 532 nm at three different levels of strength, i.e., 0, 1, or 2 W/cm^2 (Verdi-V10, COHERENT, Santa Clara, CA, USA). The temperature of the AuNP-hydrogel(cg) was monitored using a contact thermometer (TT-508, TANITA, Tokyo, Japan).

[5] Evaluation of Laser-responsive Disruption of AuNP-hydrogel

AuNP-hydrogel(cg) in PBS was exposed to laser irradiation at 532 nm at 1-2 W/cm^2 (Compass 315M-100). Supernatants were periodically sampled for the evaluation of the disruption of the hydrogel. The structure of released products was assessed by PAGE analysis after staining with

SYBR Gold (Molecular Probes, Eugene, OR, USA). The amounts of released components, i.e., DNA and AuNP, were determined by using NanoDrop 2000 spectrophotometer by measuring the absorbance at 260 and 532 nm, respectively.

[6] Cell Culture

Murine macrophage-like RAW264.7 cells were cultured in RPMI medium supplemented with 10% heat-inactivated FBS, 0.2% sodium bicarbonate, 100 IU/mL penicillin, 100 μg/mL streptomycin and 2 mM L-glutamine. Murine dendritic DC2.4 cells (kindly provided by Dr. K. L. Rock, University of Massachusetts Medical School, Worcester, MA, USA) were cultured in RPMI medium supplemented with 10% heat-inactivated FBS, 0.2% sodium bicarbonate, 100 IU/mL penicillin, 100 μg/mL streptomycin, 2 mM L-glutamine, 0.5 mM monothioglycerol and 0.1 mM non-essential amino acids. These cells were plated on 96-well culture plates at a density of 5×10^4 cells/well, and cultured for 24 h prior to use.

[7] *In Vitro* Cytokine Release

Samples in test tubes were irradiated with laser at 532 nm at 2 W/cm^2. The supernatant of the irradiated samples was collected, serially diluted with PBS, and added to cultured RAW264.7 cells. After 16 h of incubation at 37°C, culture supernatants were collected for enzyme-linked immunosorbent assay (ELISA). The levels of mouse tumor necrosis factor (TNF)-α and interleukin (IL)-6 were determined using OptEIA™ sets (Pharmingen, San Diego, CA).

[8] Statistical Analysis

Differences were statistically evaluated by one-way analysis of variance followed by Fisher's LSD for multiple comparisons. P values of less than 0.05 were considered statistically significant.

Table 2: The Sequences of ODNs Used for Preparation of Nanoassemblies

ODN	Sequence (5′→3′)	Nanoassembly
ODN(cg)-polyA	cgtcagga gacgtttgtg aaaaaaaaaaaa	AuNP-ODN(cg)-A
Hexapodna(cg)-A-#1	tcctgacg ttgctagacgctgtca gcacgtcgtagtgcaa	hPODNA(cg)-A
Hexapodna(cg)-A-#2	tcctgacg ttgcactacgacgtgc agcagacgtcgatcaa	
Hexapodna(cg)-A-#3	tcctgacg ttgatcgacgtctgct tgacgctcagctgcaa	
Hexapodna(cg)-A-#4	tcctgacg ttgcagctgagcgtca gacgctgatctagcaa	
Hexapodna(cg)-A-#5	tcctgacg ttgctagatcagcgtc ctcacgttgactacaa	
Hexapodna(cg)-A-#6	tcctgacg ttgtagtcaacgtgag tgacagcgtctagcaa	
Hexapodna(cg)-B-#1	cgtcagga cgttgaatccatgacg ttgtatgactgcaacg	hPODNA(cg)-B
Hexapodna(cg)-B-#2	cgtcagga cgttgcagtcatacaa tcctgacgctctgacg	
Hexapodna(cg)-B-#3	cgtcagga cgtcagagcgtcagga cgttcatcagtatacg	
Hexapodna(cg)-B-#4	cgtcagga cgtatactgatgaacg aagtgacgtctcaacg	
Hexapodna(cg)-B-#5	cgtcagga cgttgagacgtcactt atcgacgtctgagacg	
Hexapodna(cg)-B-#6	cgtcaingga cgtctcagacgtcgat cgtcatggattcaacg	
ODN(gc)-polyA	gctcagga tggcattgtg aaaaaaaaaaaa	[AuNP-ODN(gc)-A]
Hexapodna(gc)-A-#1	tcctgagc ttgctagagcctgtca ggagcagctagtgcaa	hPODNA(gc)-A
Hexapodna(gc)-A-#2	tcctgagc ttgcactagctgctcc agcagagctcgatcaa	
Hexapodna(gc)-A-#3	tcctgagc ttgatcgagctctgct tgagcctcagctgcaa	
Hexapodna(gc)-A-#4	tcctgagc ttgcagctgaggctca gagcctgatctagcaa	
Hexapodna(gc)-A-#5	tcctgagc ttgctagatcaggctc ctcagcttgactacaa	
Hexapodna(gc)-A-#6	tcctgagc ttgtagtcaagctgag tgacaggctctagcaa	
Hexapodna(gc)-B-#1	gctcagga gcttgaatccatgagc ttgtatgactgcaagc	hPODNA(gc)-B
Hexapodna(gc)-B-#2	gctcagga gcttgcagtcatacaa tcctgagcctctgagc	
Hexapodna(gc)-B-#3	gctcagga gctcagaggctcagga gcttcatcagtatagc	
Hexapodna(gc)-B-#4	gctcagga gctatactgatgaagc aagtgagctctcaagc	
Hexapodna(gc)-B-#5	gctcagga gcttgagagctcactt atgcagctctgagagc	
Hexapodna(gc)-B-#6	gctcagga gctctcagagctgcat gctcatggattcaagc	

Table 3: Nanocomposites and their Components Used in Each Experiment

Nanocomposite	Component A	Component B	Fig. 14a	Fig. 14 b, c	Fig, 15a	Fig. 15b	Fig. 16a, d	Fig. 16b, c	Fig. 17,
AuNP-hydrogel(cg)	AuNP-ODN(cg)-A	hPODNA(cg)-B	X	X	X	X	X	X	X
AuNP-hydrogel(gc)	AuNP-ODN(gc)-A	hPODNA(gc)-B	X						X
AuNP-ODN/hPODNA(cg)	AuNP-ODN(cg)-A	hPODNA(cg)-A	X		X			X	
AuNP-ODN/hPODNA(gc)	AuNP-ODN(gc)-A	hPODNA(gc)-A	X						
Hydrogel(cg)	hPODNA(cg)-A	hPODNA(cg)-B			X			X	X
Hydrogel(gc)	hPODNA(gc)-A	hPODNA(gc)-B							X
AuNP(cg)	AuNP-ODN(cg)-A	-			X				X
AuNP(gc)	AuNP-ODN(gc)-A	-							X

2.3 Results

2.3.1 Synthesis of AuNP-DNA Nanocomposites and their Appearance

To synthesize the hydrogel as AuNP-DNA nanocomposites, two types of building blocks, i.e., AuNP-ODNs and hexapodnas, were prepared, separately.

<AuNP-ODNs>

AuNPs with diameter of 50 nm were used based on the previous report that AuNPs of this size efficiently delivered CpG DNA to lymph nodes *in vivo*[88]. Following the method previously reported[87], ODNs with polyadenine sequence were mixed with AuNPs under citrate-buffered low-pH conditions. In agarose gel electrophoresis, red bands were detected for the mixture of AuNPs and the ODNs, whereas a purple band with lower mobility was obtained for AuNPs (Figure 12 (b)). It was in accordance with results previously reported[87], which suggested that ODNs were successfully adsorbed onto AuNPs to obtain AuNP-ODNs conjugate (AuNP-ODN(cg)-A、AuNP-ODN(cg)-B).

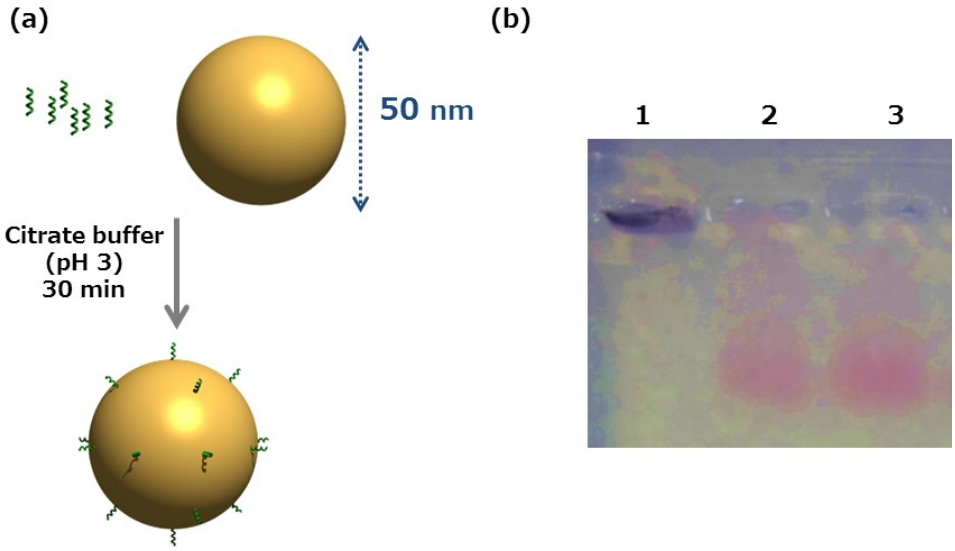

Figure 12: Preparation of AuNP-ODNs. (a) Schematic illustration of modification of AuNP with ODNs. ODNs with polyadenine sequence were adsorbed onto surface of AuNPs by mixing in citrate-buffered low-pH conditions as previously reported[87]. (b) Agarose gel electrophoresis of AuNP and AuNP-ODNs conjugate. Each sample was run on an agarose gel at 150 V for 60 min. lane 1, AuNP: lane 2, AuNP-ODN(cg)-A, lane 3, AuNP-ODN(cg)-B.

<Hexapodnas>

Four types of hexapodnas, i.e., hPODNA(cg)-A, hPODNA(gc)-A, hPODNA(cg)-B, and hPODNA(gc)-B, were prepared by mixing equimolar six ODNs for each preparation. PAGE analysis indicated that hexapodnas were successfully prepared (Figure 13).

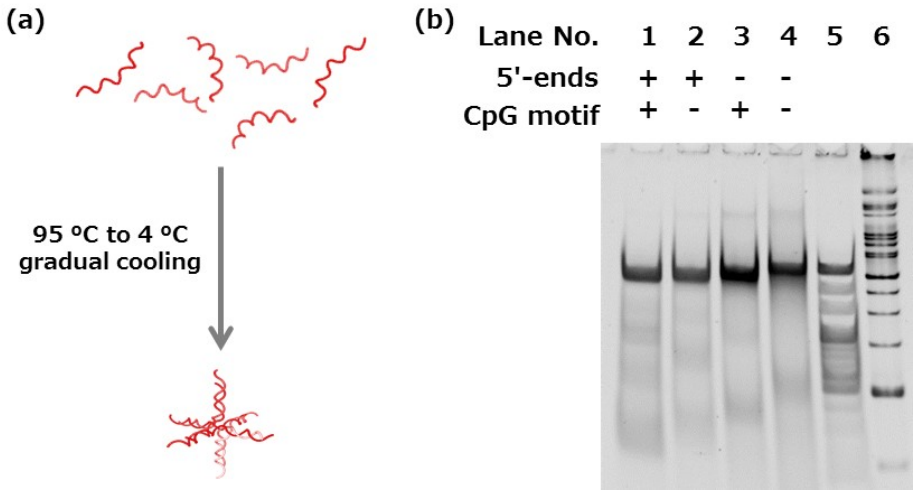

Figure 13: Preparation of Hexapodnas. (a) Schematic illustration of hexapodna formation. Hexapodna was prepared by annealing equimolar mixture of six different ODNs with the halves of each ODN being partially complementary to the halves of the other two ODNs. (b) PAGE analysis of hexapodna formation. Each samples was run on a polyacrylamide gel at 200 V for 20 min. lane 1, hPODNA(cg)-B; lane 2, hPODNA(gc)-B; lane 3, hPODNA(cg)-A; lane 4, hPODNA(gc)-A; lane 5, 20 bp ladder; lane 6, 100 bp ladder.

< AuNP-DNA Nanocomposites >

It was designed that AuNP-DNA nanocomposite would form by mixing of hexapodnas and other components with the 5'-ends complementary to the sequence of the hexapodnas. To examine this, hexapodnas and AuNP-ODNs with the 5'-ends complementary or non-complementary sequences were mixed. When AuNP-ODN(cg)-A and hPONDA(cg)-B were mixed together, viscous droplets were obtained (Figure 14 (a), right). Such viscous droplets were not obtained by mixing AuNP-ODN(cg)-A and hPODNA(cg)-A (Figure 14 (a), left, AuNP-ODN/hPODNA(cg)). It suggested that interactions between the complementary sequences of AuNP-ODN(cg)-A and hPONDA(cg)-B result in the formation of a viscous hydrogel, which was named as AuNP-hydrogel(cg). Scanning electron microscope imaging showed that the AuNP-hydrogel(cg) had a well-ordered structure, and the AuNPs distributed uniformly within the structure (Figure 14 (b), (c)). Use of AuNP-ODN and hexapodna containing GpC sequences instead of CpG ones produced similar results (data not shown).

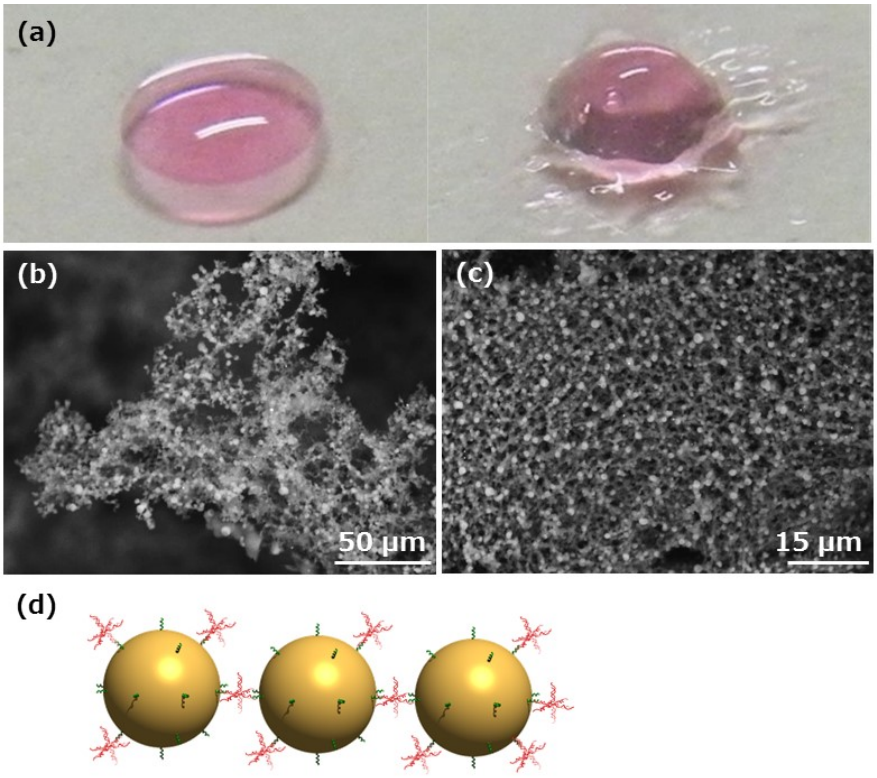

Figure 14: Appearance of AuNP-DNA Nanocomposite. (a) Optical image of AuNP-DNA nanocomposites. (Left) A droplet of the mixture of AuNP-ODN(cg)-A and hPODNA(cg)-A (AuNP-ODN/hPODNA(cg)). (Right) A droplet of the mixture of AuNP-ODN(cg)-A and hPODNA(cg)-B (AuNP-hydrogel(cg)). (b-c) SEM images of AuNP-hydrogel(cg). Images were taken using a scanning electron microscope at three different magnifications (b) × 1800; (c) × 2000. (d) Schematic illustration of hydrogel formation mechanism.

2.3.2 Photothermal Activity of AuNP-DNA Nanocomposite

Figure 15 (a) shows the UV-visible absorbance spectra of hydrogel(cg), AuNP, AuNP-ODN/hPODNA(cg), and AuNP-hydrogel(cg). All the samples containing AuNPs, i.e., AuNP, AuNP-ODN/hPODNA(cg), and AuNP-hydrogel(cg), had quite similar spectra with a peak around 532 nm, indicating that the DNA surrounding AuNPs had no significant impact on the surface plasmon resonance effects of AuNPs. To evaluate the photothermal behaviors of the AuNP-hydrogel(cg), the temperature profile was monitored under laser irradiation (Figure 15 (b)). When the laser irradiation was initiated, the temperature of AuNP-hydrogel(cg) was promptly increased, and reached plateau in about 180 sec. The temperature quickly decreased upon cessation of the irradiation. The increasing rate of the temperature and the plateau level were dependent on the laser strength. Irradiation at 2 W/cm^2 increased the

temperature from 27 °C (room temperature) to 46 °C in 60 sec.

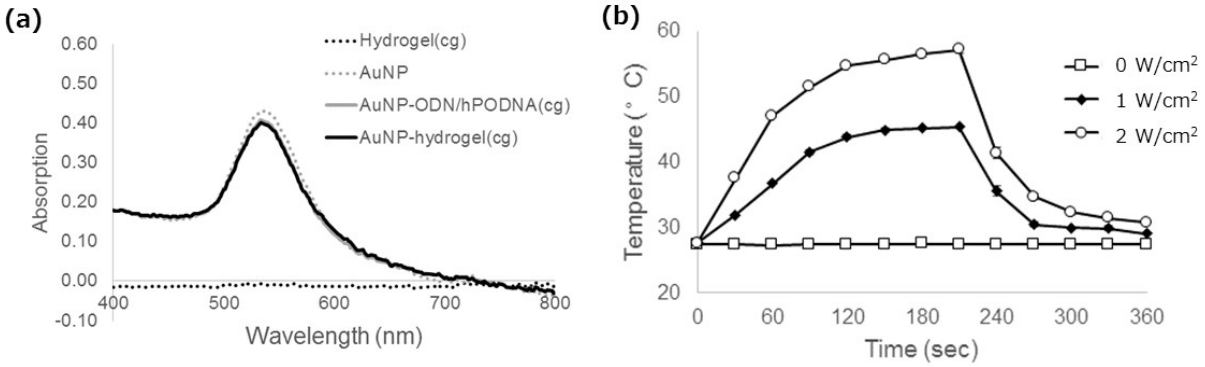

Figure 15 : Photothermal Properties AuNP-DNA. (a) UV-visible absorbance spectra of AuNP-DNA nanocomposites and their components. UV-visible spectra of hydrogel(cg), AuNP, AuNP-ODN/hPODNA(cg), and AuNP-hydrogel(cg) were recorded using NanoDrop 2000 spectrophotometer. (b) Photothermal behavior of the AuNP-hydrogel(cg) in response to laser irradiation. The temperature was monitored using contact thermometer. Data are expressed as the mean ± S.D. of three independent samples. Open square, 0 W/cm^2; Closed diamond, 1 W/cm^2; Open circle, 2 W/cm^2.

2.3.3 Laser-induced Disintegration of AuNP-hydrogel(cg)

To evaluate the behavior of AuNP-DNA nanocomposite under laser irradiation, AuNP-hydrogel(cg) was illuminated by laser. When the laser was irradiated, the hydrogel was immediately disrupted. In contrast, the appearance of AuNP-hydrogel(cg) hardly changed without laser irradiation (Figure 16 (a)). To examine the release profiles of DNA and AuNP from AuNP-hydrogel(cg), AuNP-ODN/hPODNA(cg), and hydrogel(cg), DNA and AuNP were determined by spectrophotometer in the absorbance at 260 and 532 nm, respectively (Figure 16 (b)-(c)). Without laser irradiation, no detectable DNA or AuNP were released from AuNP-hydrogel(cg) and hydrogel(cg), the latter of which is a hexapodna-based DNA hydrogel containing no AuNPs. Laser irradiation induced an immediate release of both DNA and AuNPs from AuNP-hydrogel(cg), whereas no DNA was released from hydrogel(cg) upon laser irradiation, indicating the importance of AuNP on the laser-irradiated release of DNA. On the other hand, AuNP-ODN/hPODNA(cg) showed slow release of DNA and AuNPs irrespective of laser irradiation.

It has been previously demonstrated that constructing DNAs into highly ordered

structure played a key role for efficient CpG DNA delivery to immune cells[30]. To address the structures of released DNAs, sampled aliquots were analyzed using PAGE. Mild laser irradiation at 1 W/cm^2 for 3 min or at 2 W/cm^2 for 1-2 min generated low mobility bands (Figure 16 (a), lanes 2-4), suggesting the dissociation of AuNP-ODN and hexapodna. On the other hand, strong laser irradiation at 2 W/cm^2 for 5 min or 3 min generated high mobility bands (Figure 16 (a), lanes 5, 6), which suggests that these laser conditions degraded hexapodna into ODNs. However, AuNP-ODN interaction seemed not to be dissociated even under these conditions, because no bands corresponding to free AuNP were detected.

It was considered that this unique disruption property was brought by the differences in thermal stability between the components of nanoassemblies themselves and interactions in their complementary adhesive ends. The designated melting temperature (Tm) of the 8-mer 5′-adhesive ends is calculated to be approximately 35°C. On the other hand, the estimated Tm of 32-mer hexapodna body is approximately 70°C at a DNA concentration of 500 μmol/mL. Moreover, a previous report showed that the AuNP-ODN interaction was stable even at 95°C[87].

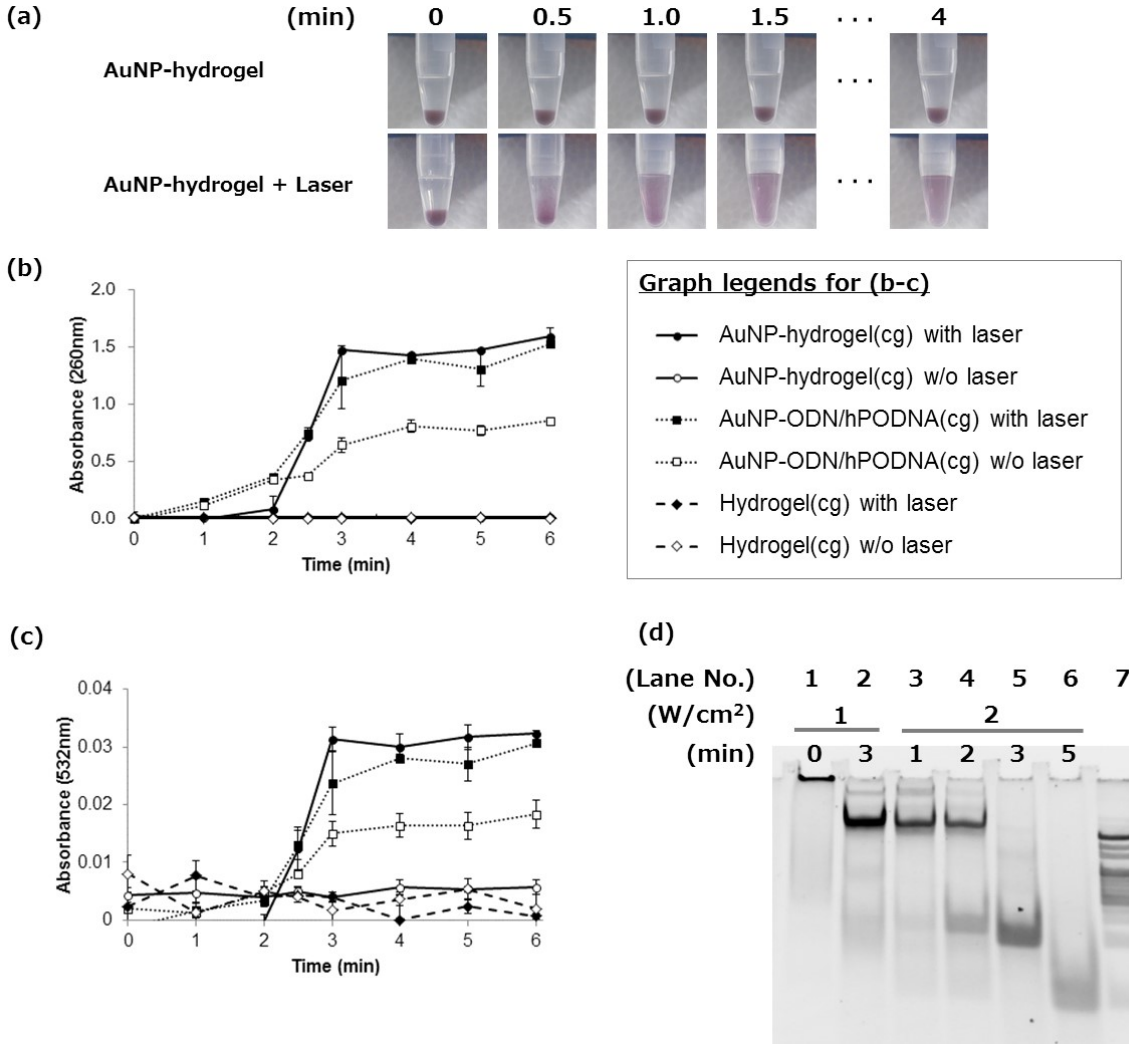

Figure 16 : **Laser-induced Disintegration of AuNP-hydrogel(cg).** (a) Laser-induced disintegration of AuNP-hydrogel(cg). AuNP-hydrogel(cg) in PBS was irradiated with laser at 2 W/cm^2 for 1 min. At indicated time points, laser was tuned off and optical images were recorded. (b-c) Release profile of the components from AuNP-hydrogel(cg), AuNP-ODN/hPODNA(cg) and hydrogel(cg). Each composite in PBS was irradiated with laser at 2 W/cm^2 for 1 min. At indicated time points, laser was tuned off, and samples were collected from the top of the solution. The concentration of ODN and AuNPs were measured by absorbance at wavelength of 260 nm and 532 nm, respectively, using NanoDrop 2000 spectrophotometer. Results are expressed as the mean ± S.D. of three independent samples. (d) PAGE analysis of the released products from AuNP-hydrogel(cg) with or without laser irradiation. Each sample was run on a 10% polyacrylamide gel at 150 V for 60 min. Lane 1, 20 bp DNA ladder; lane 2, 2 W/cm^2 for 5 min; lane 3, 2 W/cm^2 for 3 min; lane 4, 2 W/cm^2 for 2 min; lane 5, 2 W/cm^2 for 1 min; lane 6, 1 W/cm^2 for 3 min; lane 7, no irradiation.

2.3.4 Immunostimulatory Activity of AuNP-DNA Nanocomposite

The immunostimulatory activity of the components of AuNP-DNA nanocomposite was examined using mouse macrophage-like RAW264.7 cells. Both hexapodna and AuNP-ODN containing CpG motif induced TNF-α release from RAW264.7 cells, whereas those with GpC did not. Forming AuNP-DNA hydrogel containing CpG motifs significantly increased TNF-α release (Figure 17). To address the mechanism of this increased immunostimulatory activity, the uptake of DNA in RAW264.7 cells was evaluated by using fluorescent Cy-5 labeled ODNs. Enhanced cellular uptake was observed when the AuNP-ODN, a conjugate of AuNP and ODNs, was added compared to physical mixture of AuNP and ODNs (Figure 18).

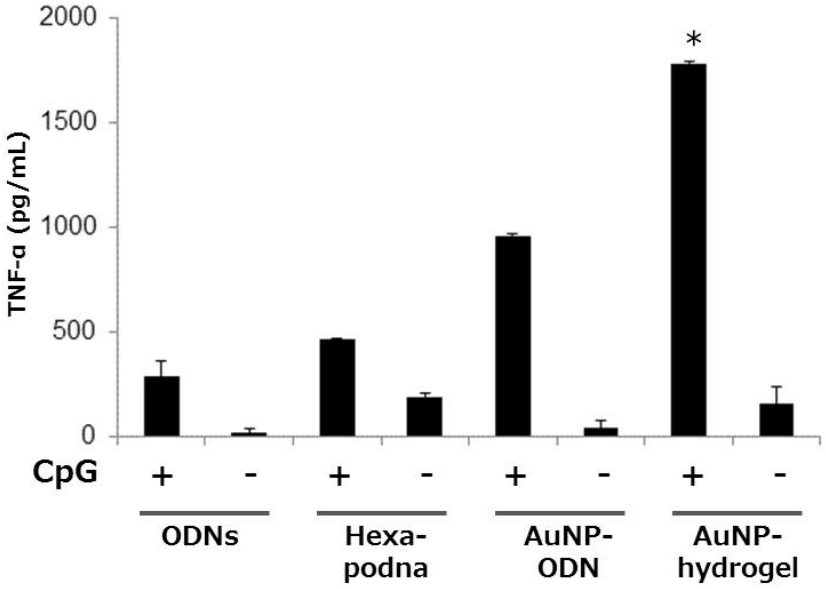

Figure 17 : Immunostimulatory Activity of Components of AuNP-DNA Nanocomposite. Cells were incubated with DNA samples for 16 hr. The TNF-α concentration in culture media was determined by ELISA. 1, AuNP-ODN/hPODNA(cg); 2, AuNP-ODN/hPODNA(gc); 3, AuNP(cg); 4; AuNP(gc); 5, Hydrogel(cg); 6, Hydrogel(gc); 7, AuNP-hydrogel(cg); 8, AuNP-hydrogel(gc). Results are expressed as the mean ± S.D. of three independent wells per sample. Data shown are representative of three independent experiments. *P < 0.05 compared with other groups.

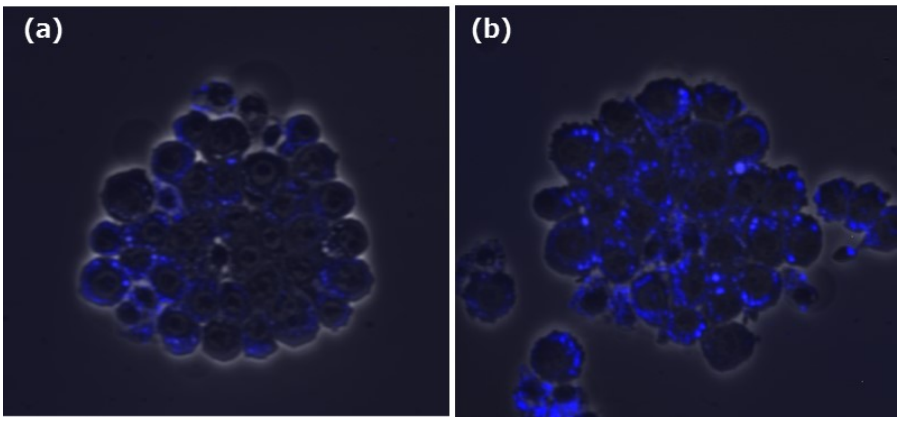

Figure 18 : Effect of Conjugating AuNP-ODN on CpG DNA Uptake by RAW264.7 Cells. Cy5-labeled DNA sample in Opti-MEM was added to cells at a final concentration of 1.2 nM, and cells were incubated for 8 h at 37 °C. Typical images of RAW264.7 cells after addition of Cy5-labeled (a) physical mixture of AuNP and ODNs, (b) AuNP-ODN conjugate.

Moreover, to investigate the laser responsiveness of the immunostimulatory activity, the products released by laser irradiation was sampled at each time points, and their effects on the cytokine release from immune cells were evaluated. Figure 19 (a)-(d) show that both mouse dendritic DC2.4 cells and mouse macrophage-like RAW264.7 cells released TNF-α and IL-6 only when added with the supernatants of the laser irradiated AuNP-DNA hydrogel(cg).

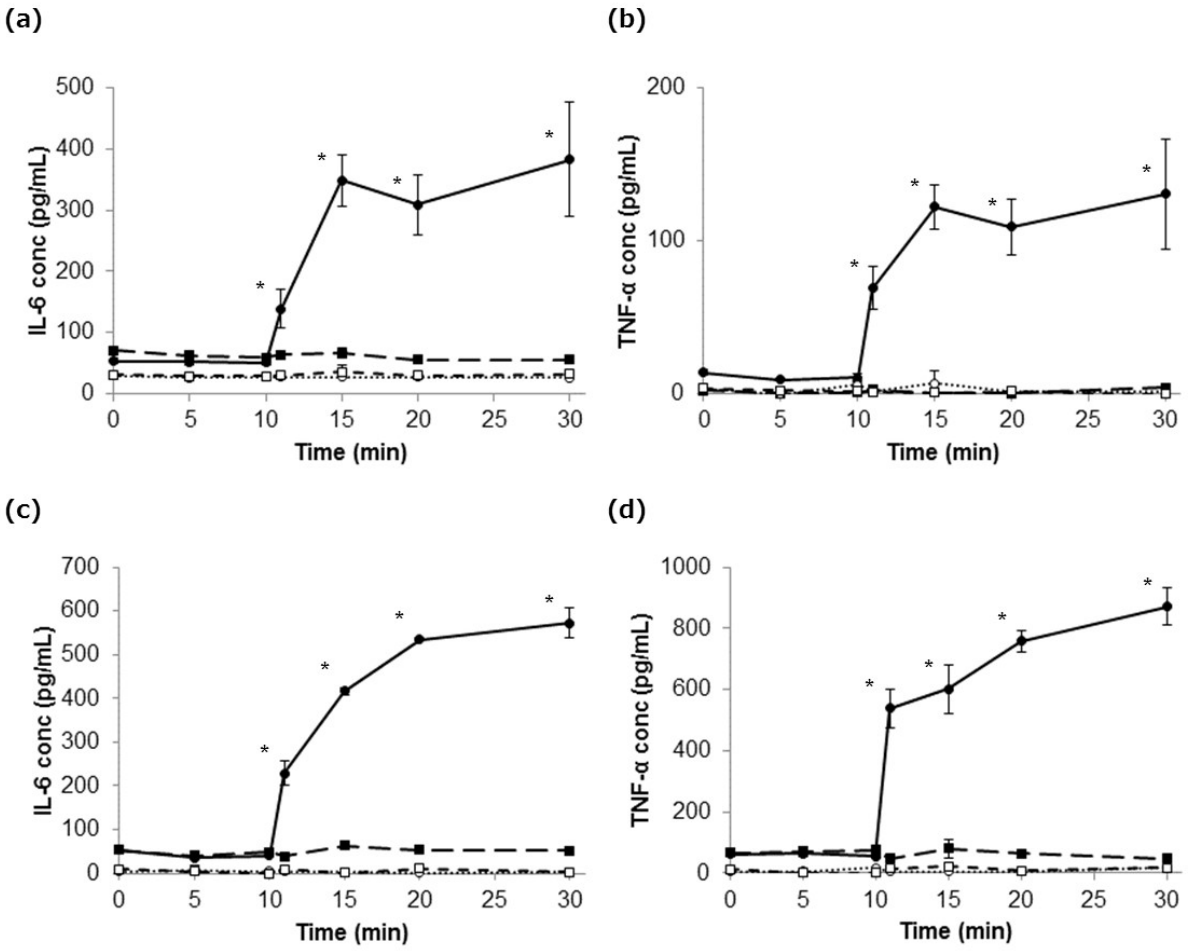

Figure 19 : Immunostimulatory Activity of AuNP-DNA Nanocomposite. (a) IL-6 release from DC2.4 cells. (b) TNF-α release from DC2.4 cells. (c) IL-6 release from RAW264.7 cells. (d) TNF-α release from RAW264.7 cells. DNA samples were taken from top of the solutions at the each time indicated. Cells were incubated with DNA samples at the indicated concentration for 16 hr. The concentrations of IL-6 and TNF-α in culture media were determined by ELISA. Closed circle, AuNP-hydrogel(cg) with laser irradiation; closed square, AuNP-hydrogel(cg) without laser irradiation, open circle, AuNP-hydrogel(gc) with laser irradiation; open square, AuNP-hydrogel(gc) without laser irradiation. Results are expressed as the mean ± S.D. of three independent wells per sample. Data shown are representative of three independent experiments. *P < 0.05 compared with other groups.

2.4 Discussion

In this study, to prepare a composite-type hydrogel from AuNP and polypodna, "self-gelling nucleic acid" technology was applied with expanding from inter-polypodnas to inter-different nanoassemblies. The designed nanocomposite consisting of AuNP-ODN and hexapodna with complementary 5'-ends each other formed a viscous hydrogel, named AuNP-DNA hydrogel(cg) (Figure 14). The AuNP-hydrogel(cg) showed photothermal activity, and produced heat in laser responsive manner derived from the surface plasmon resonance of AuNPs (Figure 15 (a)). Tuned laser irradiation was able to immediately increase the temperature of AuNP-hydrogel(cg) to reach a target temperature for the photothermal immunotherapy of approximately 45°C (Figure 15 (b)). The AuNP-hydrogel(cg) was disrupted at around 45°C to release its components (Figure 16 (a)). The structures of released ODNs were different depending on the laser irradiation levels (Figure 16 (b)). PAGE analysis suggested that under the tuned irradiation (2 W/cm^2 for 1 min or 1 W/cm^2 for 3 min) the AuNP-hydrogel(cg) could release hexapodna and AuNP-ODN without losing their highly ordered structure which played a key role for efficient CpG DNA delivery to immune cells (Figure 16 (c)). In fact, the AuNP-hydrogel(cg) was able to activate mouse macrophage-like RAW264.7 cells and mouse dendritic cells DC2.4 to produce released TNF-α and IL-6 through efficient delivery of CpG motif to these immune cells (Figure 17, Figure 19).

Previous studies have reported generation of laser responsiveness to DNA-based hydrogel by hybridizing DNA hydrogel and gold nanoparticles[89, 90]. The AuNP-hydrogel(cg) of the present study can be considered to be safer than those previously reported DNA-based hydrogels from the view of medical applications. It is because the AuNP-hydrogel(cg) could be prepared through "self-gelling nucleic acid" without chemical bonding or ligation processes, and have low risk of impurities. Moreover, since the compounding process did not assure a uniformity in the inner structure, there is little potential risk for variations in heat irradiation. Actually, it was shown that the AuNP-hydrogel(cg) had highly ordered inner structure (Figure 14).

In conclusion, an injectable, photothermally active, and immunostimulatory hydrogel formulation was developed by hybridize AuNP and hexapodna through "self-gelling nucleic acid" technology.

Chapter 2-2 : Development of Hydrogel Formulation for *In Vivo* Application

2.5 Introduction

To develop a hydrogel formulation applicable to *in vivo* photothermal immunotherapy, it is essential for hydrogel formulation to be responsive in laser irradiated from outside of the body. It was demonstrated that the AuNP-hydrogel(cg) possessed both photothermal and immunostimulatory activity as designed. However, all of these responses were based on the laser irradiation at wavelength of 532 nm, which is disturbed by skin, subcutaneous tissues, hemoglobin, and other biological components. Although to use a stronger laser to deliver photothermal activity *in vivo* can be an option, it would be dangerous and costly for clinical applications. It is, therefore, a reasonable option to shift the absorbance wavelength by using other photosensitizers than the AuNPs used in the previous chapter. Gold nanorods (AuNRs), another kind of gold nanoparticles, allow to shift absorption peaks to the biological window of 650-900 nm. In this study, AuNR-DNA hydrogel(cg), in which AuNR is used as a sensitizing agent in replacement of AuNP, was synthesized, and evaluated its applicability to *in vivo* photothermal immunotherapy.

2.6 Methods

[1] Preparation of AuNR-hydrogel

AuNRs with a dimensions of 38 nm by 10 nm were purchased from Sigma-Aldrich (St. Louis, MO, USA). All ODNs were purchased from Integrated DNA Technologies, Inc. (Coralville, IA, USA). The sequences of the ODNs used are summarized in Table 4. To prepare ODN-modified AuNR, a CpG ODN with polyadenine sequence was adsorbed onto the surface of AuNPs as the same manner as in Chapter 2.1. Separately, hexapodna containing complementary 5'-ends with ODNs on AuNR was prepared by mixing equimolar six ODNs for each preparation as described in Chapter 2.1.

[2] Animals

Five-week-old female C57BL6/J mice were purchased from Japan SLC, Inc. (Shizuoka, Japan). All protocols for the animal experiments were approved by the Animal Experimentation Committee of the Graduate School of Pharmaceutical Science of Kyoto University. The animal experiments were carried out in accordance with EC Directive 86/609/EEC.

[3] Photothermal Activity *In Vivo*

Under anesthetization, 100 μg (as DNA) of AuNR-hydrogel(cg), 100 μg (as DNA) of AuNR/ODNs mixture, and saline in a volume of 50 μL was injected intratumorally in C57BL/6 mice. Mice of three groups with different agents injected were irradiated with an NIR laser (Femtosecond Titanium Sapphire laser Chameleon-RF; Coherent, Santa Clara, CA, USA) at 780 nm. During irradiation, temperature was monitored using thermography (testo890, TESTO AG, Lenzkirch, Germany).

[4] Hsp70 mRNA Determination

Total RNA from tumor tissues was extracted using Sepasol-RNA I Super (Nacalai Tesque, Inc., Kyoto, Japan) and was reverse transcribed to cDNA using a ReverTra Ace qPCR RT Master Mix with gDNA Remover (TOYOBO Co., Ltd., Osaka, Japan). Real-time PCR was performed on a LightCycler (Roche Diagnostics, Basel, Switzerland) with a LightCycler FastStart DNA MasterPLUS SYBR Green I kit (Roche Diagnostics KK, Tokyo, Japan). PCR amplification was performed as follows: 10 min at 95°C, 50 cycles of 10 s at 95°C, 5 s at 56°C and 15 s at 72°C. The oligonucleotide primers used for amplification were as follows: Hsp70, forward, 5'-GGCCAGGGCTGGATTACT-3′ and reverse, 5'-GCAACCACCATGCAAGATTA-3'; β-actin, forward, 5′-CATCCGTAAAGACCTCTATGCCAAC-3′, and reverse, 5′-ATGGAGCCACCGATCCACA-3′. After PCR was completed, the LightCycler software (Roche Diagnostics) converted the raw data into copies of target molecules. The mRNA expression of target genes was normalized by using the amount of β-actin mRNA.

[5] Measurement of OVA-specific Antibody Production

Serum samples were serially diluted to measure the OVA-specific total IgG levels by ELISA as previously reported[91]. One hundred milligram per milliliter OVA in carbonate/bicarbonate buffer (0.1 M, pH 9.6) was distributed to each well of 96-well flat-bottom polystyrene plates (100 μL per well). Following overnight incubation at 4°C, wells were blocked with 5% BSA-containing Tween-20-phosphate buffered saline (T-PBS) [0.5%, w/w, Tween-20 (ICN Biomedicals Inc. Aurora, OH, USA) in PBS] for 30 min at 37°C. After the wells were washed three times with T-PBS, serially diluted 100 μL serum samples were added to the wells. After 2 h incubation at 37°C, the wells were washed five times with T-PBS and 100 μL anti-IgG-horseradish peroxidase (HRP) conjugate, diluted 2000:1 with 5% BSA-containing T-PBS, was added to each well. After a 2 h incubation, each well was washed with T-PBS and then 200 μL freshly prepared o-phenylenediamine dihydrochloride solution in phosphate-citrate buffer (0.05 M, pH 5.0) was add to each well. After a 30 min incubation, 50

μL 10% H_2SO_4 was added and then the absorbance was measured at 490 nm. Serum total IgG titers were estimated by the dilution ratio at which absorbance value of 0.1 was obtained.

[6] IFN-γ Secretion from Splenocytes

Fourteen days after the last treatment, splenocytes were isolated, purified, and cultured in the presence of OVA (1 mg/mL) in 12 well culture plate for 2 days. Concentration of IFN-γ in supernatant of the cultured cells was determined by ELISA (Ready-SET-Go! Mouse IFN-γ ELISA, eBioscience, San Diego, CA, USA) as previously reported[34].

[7] Treatment of Tumor-bearing Mice

C57BL/6 mice were inoculated with EG7-OVA cells (6×10^6 cells/mouse) intradermally on the back. When the tumor volume exceeded 200 mm^3, 100 μg (as DNA) of AuNR-hydrogel(cg), 100 μg (as DNA) of AuNR/ODNs mixture, and saline in a volume of 50 μL was injected directly into the tumor under anesthesia with sodium pentobarbital (Nacalai Tesque, Kyoto, Japan). After the intratumoral injection, the mice of three groups with different agents injected were irradiated with an NIR laser (Femtosecond Titanium Sapphire laser Chameleon-RF; Coherent, Santa Clara, CA) at 780 nm. The parameters for the NIR laser treatment were set to 3-min and 1.0 W. After the treatment, the tumor size was measured with a slide caliper every days for 14 days, and the tumor volume was calculated using the following formula: tumor volume (mm^3) = 0.5 × length (mm) × [width (mm)]^2 .

[8] Statistical Analysis

Differences were statistically evaluated by one-way analysis of variance followed by Fisher's LSD for multiple comparisons. P values of less than 0.05 were considered statistically significant. To analyze the antitumor effect, Kaplan–Meier survival curves were generated, and log-rank tests were performed. P values of < 0.05 were considered significant.

Table 4: The Sequences of ODNs Used for Preparation of AuNR-hydrogel(cg)

ODN	Sequence (5'→3')	Nanoassembly
ODN(cg)-polyA	cgtcagga gacgtttgtg aaaaaaaaaaaa	AuNR-ODN(cg)
Hexapodna(cg)-A-#1	tcctgacg ttgctagacgctgtca gcacgtcgtagtgcaa	Hexapodna
Hexapodna(cg)-A-#2	tcctgacg ttgcactacgacgtgc agcagacgtcgatcaa	
Hexapodna(cg)-A-#3	tcctgacg ttgatcgacgtctgct tgacgctcagctgcaa	
Hexapodna(cg)-A-#4	tcctgacg ttgcagctgagcgtca gacgctgatctagcaa	
Hexapodna(cg)-A-#5	tcctgacg ttgctagatcagcgtc ctcacgttgactacaa	
Hexapodna(cg)-A-#6	tcctgacg ttgtagtcaacgtgag tgacagcgtctagcaa	

2.7 Results

2.7.1 Appearance of AuNR-hydrogel

For AuNR-hydrogel(cg) synthesis, the same process as for AuNP-hydrogel(cg) was applied. DNA with polyadenine sequence was adsorbed onto AuNRs under citrate-buffered low-pH conditions in the same manner as AuNPs[92]. When the hexapodna with the 5′-ends complementary sequences was mixed, the mixture formed a highly viscous hydrogel with red to purple color (Figure 20).

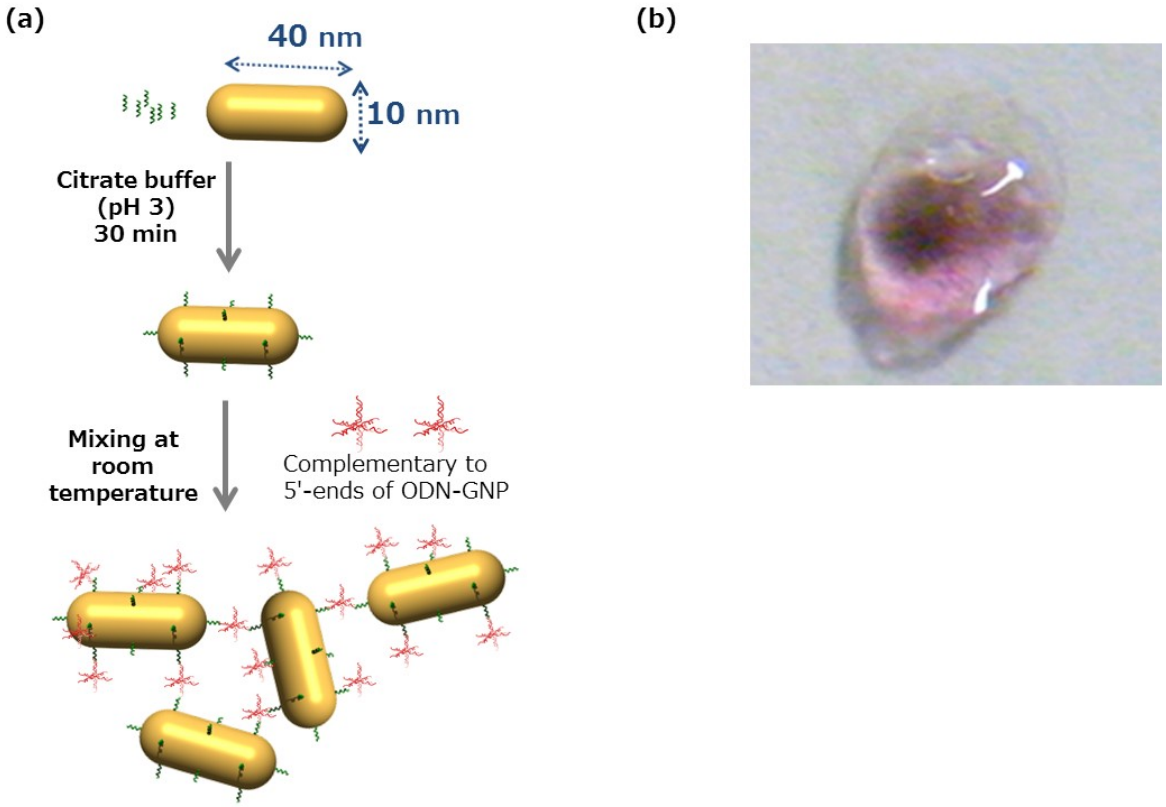

Figure 20 : Appearance of AuNR-hydrogel. (a) Schematic illustration of synthesis of AuNR-hydrogel(cg). DNA with polyadenine sequence was adsorbed onto gold nanorods in citrate-buffer with pH 3, in same manner as AuNPs. Hexapodna was prepared by mixing equimolar six ODNs. After preparing each building blocks separately, the two components were mixed at room temperature. (b) Optical image of AuNR-hydrogel(cg).

2.7.2 Photothermal Activity of AuNR-hydrogel

Figure 21 shows the ultraviolet (UV)-visible absorbance spectra of hydrogel(cg), AuNR, AuNR-ODN/hPODNA(cg), and AuNR-hydrogel(cg). As is the case of the AuNP-hydrogel, the spectra indicated that the DNA molecules surrounding AuNP had no significant impact on the surface plasmon resonance effects of AuNR. When the laser irradiation of 780 nm was initiated, the temperature of AuNR-hydrogel(cg) was promptly increased, and reached plateau in about 180 sec. The temperature quickly decreased upon cessation of the irradiation.

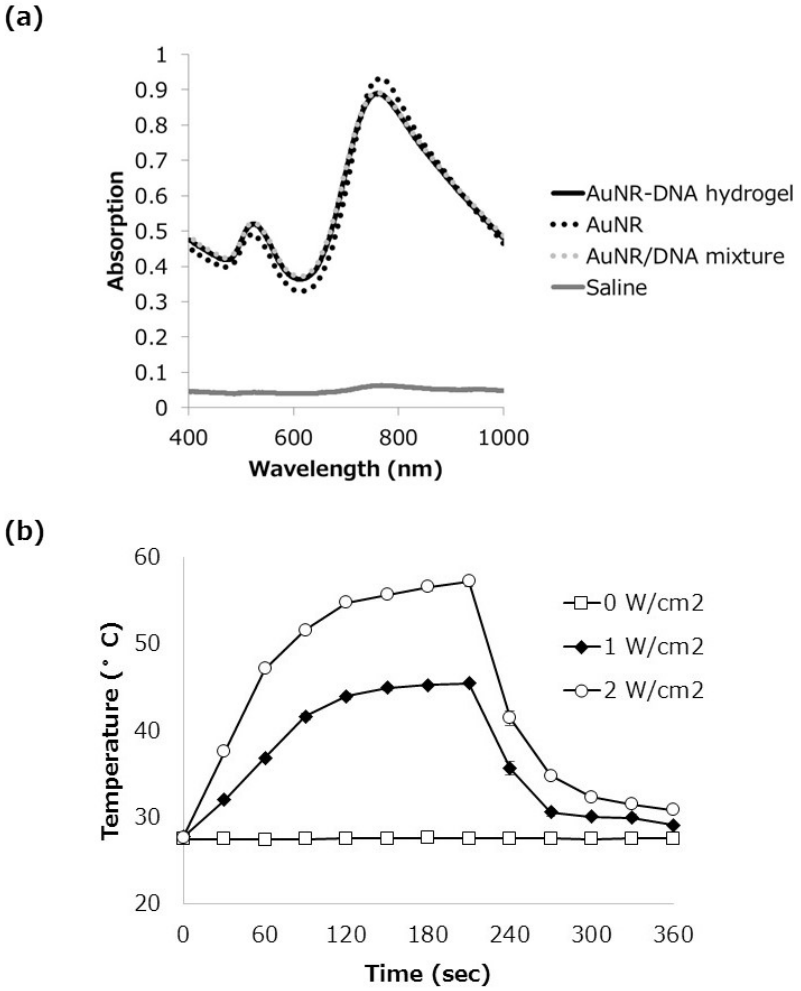

Figure 21 : Optical/Photothermal Properties of AuNR-hydrogel. (a) UV-visible absorbance spectra of AuNR-DNA nanocomposites and their components. UV-visible spectra of Saline, Hydrogel(cg), AuNR AuNR-ODN/hPODNA(cg), and AuNR-hydrogel(cg) were recorded using NanoDrop 2000 spectrophotometer. (b) Photothermal behavior of the AuNR-DNA nanocomposites in response to laser irradiation at wavelength of 780 nm. The temperature was monitored using contact thermometer.

2.7.3 Photothermal Activity of AuNR-hydrogel *In Vivo*

Photothermal control is a key for photothermal immunotherapy agents. It is necessary to control its temperature in response to laser irradiation *in vivo*. The photothermal activity of AuNR-hydrogel(cg) *in vivo* was evaluated in EG7-OVA tumor-bearing mice. Thermography showed that the temperature of the tumor injected with formulations containing AuNR, i.e., AuNR-hydrogel and AuNR/ODN, rapidly increased, but the temperature of the saline-injected tumor hardly did. The temperature reached 43 ℃, a target temperature for photothermal immunotherapy, within 45 sec. (Figure 22).

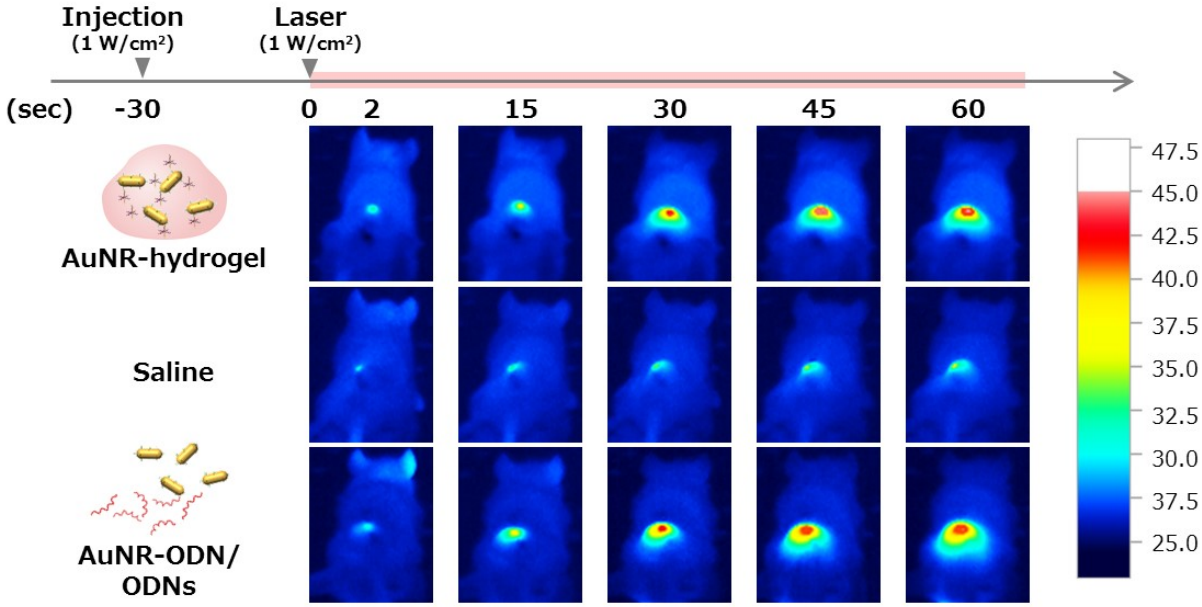

Figure 22 : **Photothermal Activity of AuNR-hydrogel.** NIR laser at the power density of 1 W/cm^2 with 780 nm wavelength was irradiated onto the back of C57BL/6 mice after subcutaneous injections of (a) AuNR-hydrogel(cg), (b) AuNR-ODN /CpG DNA or (c) saline. Temperature was monitored using thermography (testo890, TESTO AG, Lenzkirch, Germany).

2.7.4 Hsp70 mRNA Expression Levels

To evaluate the effect of AuNR-hydrogel injection plus local laser irradiation, Hsp70 mRNA levels in tumor was measured by real time PCR. The Hsp70 mRNA level significantly increased in the AuNR-hydrogel-injected and laser-irradiated mice , compared to that in the AuNR-hydrogel-injected but no laser-irradiated mice or in the saline-injected and laser-irradiated mice (Figure 23).

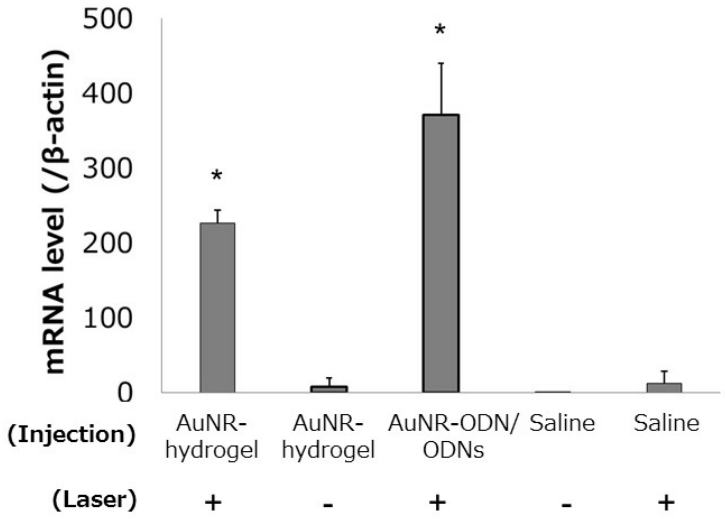

Figure 23 : HSP70 mRNA Expression Levels. The mRNA expression in the tumor tissue on postoperative day 14 is shown. Results are expressed as the mean ± S.D. of three mice. Results are typical of two separate experiments with similar results. *P < 0.05 compared with the other groups.

2.7.5 Tumor Associated Antigen Specific IgG Production

Figure 24 shows the OVA-specific total IgG production in mice 14 days after treatment. Mouse lymphoma cell line EG7 expresses OVA as a model tumor associated antigen (TAA). It is, therefore, possible to use the level of anti-OVA IgG production as an index of tumor specific humoral immune response. Mice injected with the AuNR-hydrogel showed higher IgG antibody levels than other mice. Laser irradiation did not have significant impacts on IgG production.

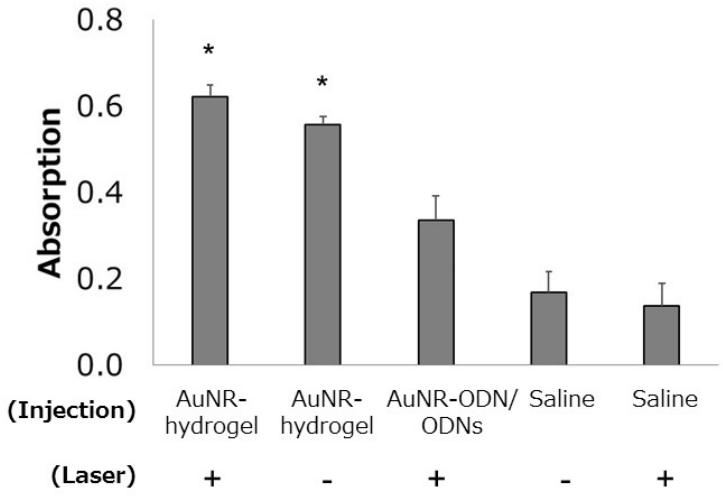

Figure 24: OVA-specific Total IgG Antibody Production in Mice. On day 14 post treatment, OVA-specific total IgG levels in serum were determined by ELISA. Serum total IgG titers were estimated by the dilution ratio at which the absorbance value of the saline group was obtained. Results are expressed as mean ± S.D. of three mice. Results are typical of two separate experiments with similar results. * $P < 0.05$ compared with the other groups.

2.7.6 Acquired Tumor Associate Antigen Specific Immune Response

To evaluate acquired antigen specific immune response in mice, IFN-γ production from splenocytes after re-stimulation with OVA was evaluated (Figure 25). Splenocytes from mice injected with the AuNR-hydrogel showed higher IFN-γ production levels compared to the others.

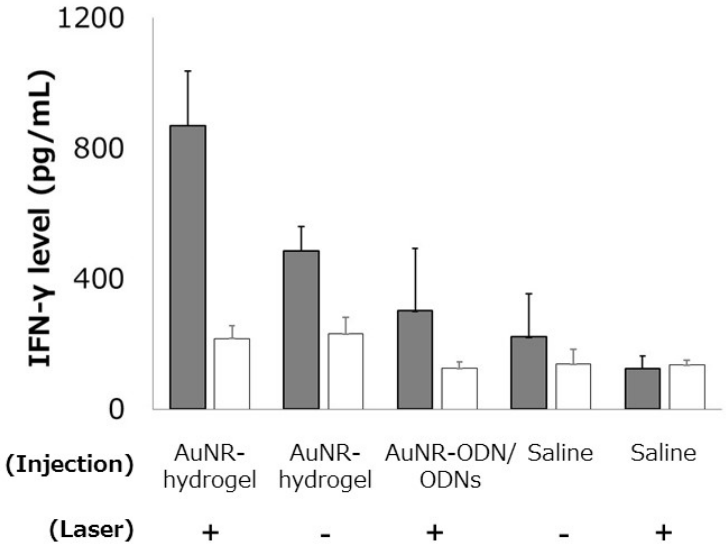

Figure 25: Interferon-γ Production from Splenocytes. On day 14 post treatment, splenocytes were collected, stimulated with OVA (1 mg/mL), and incubated for 2 d. The IFN-γ concentration in culture media was measured by ELISA. Results are expressed as mean ± S.D. of three mice. Closed bar, incubated with OVA; open bar, incubated without OVA. Results are typical of two separate experiments with similar results. * $P < 0.05$ compared with the saline group; # $P < 0.05$ compared with the groups indicated.

2.7.7 Inhibition of Tumor Growth by Photothermal Immunotherapy using AuNR-Hydrogel(cg)

The antitumor effect of photothermal immunotherapy with AuNR-Hydrogel(cg) was examined in EG7-OVA tumor-bearing mice. Figure 26 shows the tumor size and the survival rate of the tumor-bearing mice. Compared to the mice injected with saline or AuNR/ODN, tumor growth was significantly inhibited in mice injected with AuNR-hydrogel(cg), with the greatest inhibition in those receiving laser irradiation. Photothermal immunotherapy using AuNR-hydrogel(cg) also showed a significantly prolonged survival of tumor bearing mice.

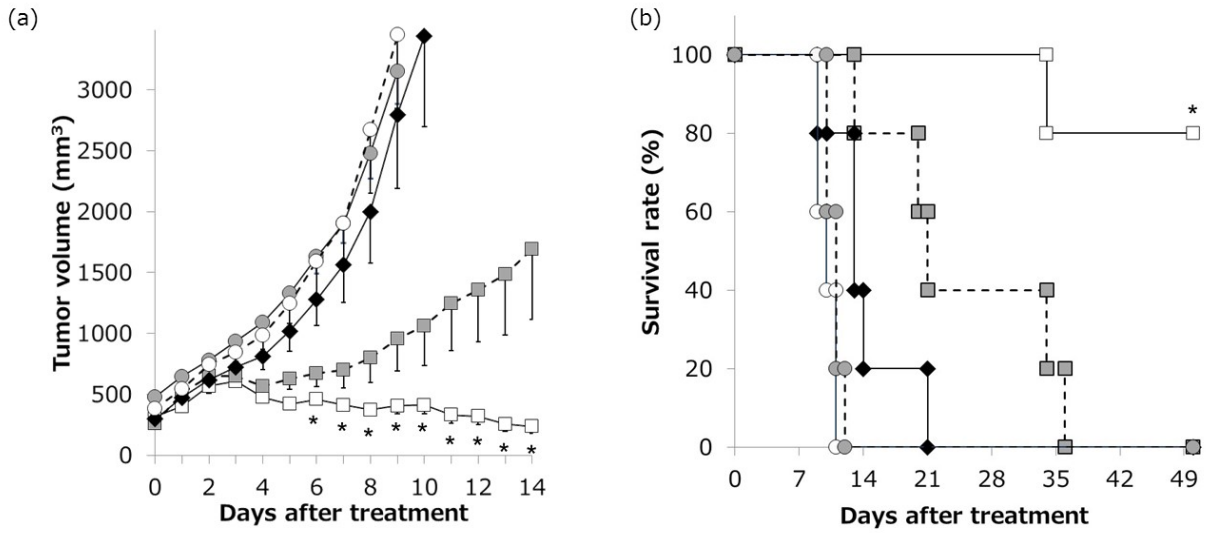

Figure 26 : **Inhibition of Tumor Growth.** EG7-OVA cells (6 × 10^6 cells) were intradermally inoculated into C57BL/6 mice. When tumor volumes reached >200 mm^3, AuNR-hydrogel(cg) (100 μg/50 μL as DNA concentration), AuNR-ODN/ CpG ODNs(100 μg/50 μL as DNA concentration), or saline (50 μL) were intratumorally injected, followed by NIR laser irradiation at the power density of 1 W/cm^2 with 780 nm wavelength. Survival (a) and tumor volume (b) were measured every day. Results are expressed as mean ± SE of eight mice (tumor volume) or five mice (survival); open square, AuNR-hydrogel(cg) with laser irradiation; gray square, AuNR-hydrogel(cg) without laser irradiation; closed diamond, AuNR-ODN/ CpG ODNs with laser irradiation; open circle, saline with laser irradiation; gray circle, saline without laser irradiation, Results are typical of two separate experiments with similar results. * $P < 0.05$ compared with the saline group.

2.8 Discussion

Photothermal immunotherapy is a new modality for tumor that well utilizes a systemic immune system raised by photothermal ablation to obtain stronger therapeutic effects. Success of this therapeutic system is highly dependent on the agents injected to induce photothermal and immunostimulatory effect in tumor. In this study, a hydrogel formulation was designed and developed as a novel booster for the photothermal immunotherapy. The composite-type hydrogel, AuNR-hydrogel(cg), demonstrated its strong photothermal activity (Figure 22) leading heat stress at the temperature of 40-45°C, which enhanced Hsp70 mRNA level in EG7-OVA tumor bearing mice (Figure 23). It enhanced the TAA specific immune responses including IgG production and TAA dependent IFN-γ release from splenocytes (Figure 24, Figure 25). Moreover, it showed a significantly strong inhibition in tumor growth rate and a prolonged survival rate (Figure 26). In a series of experiments, a group which received an injection of AuNR-ODN/DNA solution followed by laser irradiation was used for a comparison to evaluate the importance of hydrogel formulation. Although laser irradiation induced heat stress in the both groups of AuNR-hydrogel(cg) and AuNR-ODN/DNA solution, AuNR-hydrogel(cg) only exhibited high therapeutic effects, which indicated that the hydrogel formulation composed of highly ordered DNAs was able to induce stronger immune responses compared to the solution formulation.

Over the past decades, increased numbers of studies revealed the relationship between fever and immune response. It was suggested that enhanced immune reaction in response to photothermal therapy was triggered by not only increased Hsp70 levels but also by many other factors. It includes (1) increased expression of MHC class I on tumor cell surface; (2) direct activation of immune cells in tumors such as NK cells, CD8+ T cells, and DCs; (3) improvement of immune cell trafficking between the tumor and lymphoid organs. These factors might contribute to the therapeutic effects shown in this study. In addition, the superior immune induction might be brought by the hydrogel formulation. The "self-gelling nucleic acid"-based hydrogel is able to be reorganized back to hydrogel even once it melts into solution in response to an increased temperature, because the hydrogel formation is based on the hybridization between the single strand DNAs with complementary sequence. It suggests that AuNR-hydrogel(cg) was able to capture TAAs in the process of melting and hydrogel reorganization in the tumor and, thereafter, to release them in a sustained manner *in vivo* (Figure 27). It has been reported that sustained release of antigen would increase antigen-specific immune responses[93]. Incorporation of whole cells degrades as TAA by hydrogel reorganization *in situ* might be desirable from the perspective of induction of anti-tumor immune systems. Many clinical studies previously conducted around the world

have suggested that mono-molecular type of tumor vaccine including tumor-associate antigen peptide vaccine failed to show strong therapeutic effects, and that multivalent vaccine was more promising[94, 95]. Therefore, AuNR-hydrogel(cg) has a potential to be a vaccine with whole antigens from patient itself, that is, a kind of tailored-made vaccine.

This hydrogel system is promising in the view of potential to apply in further combination formulation and to provide other stimuli responsive system. Although it has not been experimentally demonstrated in this study, this hydrogel might be for use of further add-on therapy of photothermal immune-chemical combination therapy by loading drugs such as doxorubicin in the same manner as the Department has demonstrated in polypodna based DNA hydrogel previously[34]. Chad A. Mirkin et al. have reported ODNs could be conjugated with other nanoparticles such as magnetic nanoparticles, ferric oxide (Fe_3O_4) by the same mechanism as for gold nanoparticles[96]. When the photosensitizer is replaced by such other nanoparticles, it is imaginable that the hydrogel obtains other stimuli-responsiveness.

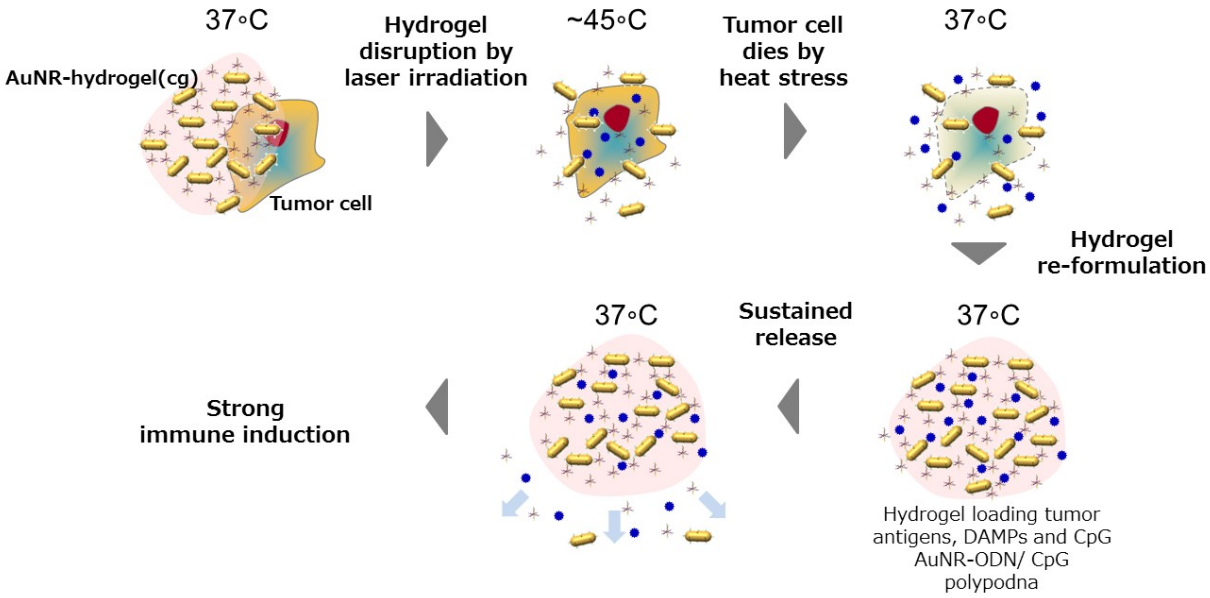

Figure 27 : Potential Mechanism as *In Situ* Forming Whole Cell Vaccine. When the temperature of AuNR-hydrogel(cg) reaches around 45 °C, the hydrogel melts by dehybridization of sticky ends to release components into cell matrix. Tumor cells around laser irradiated site come to death by heat stress. As the temperature decreases (37 °C), the components assemble again by hybridizing sticky ends, incorporating dead cells into reformed hydrogel. The hydrogel with whole cells releases antigens in sustained manner as hydrogel disintegration *in vivo*.

Conclusions

In two chapters described above, I conducted studies around self-gelling nucleic acid based DNA hydrogel.

In chapter 1, I tried to develop an efficient synthesis method for self-gelling polypod-like structured DNA to provide a solution to reduce synthesis cost in order to accelerate applying macroscale self-gelling DNA hydrogel into biomedical area. I designed a series of synthesis processes based on the combination of the rolling circle amplification and enzymatic digestion, and demonstrated that it is a practical, efficient amplification approach to obtain self-gelling DNA hydrogels in a large quantity through proof-of-concept study on amplification of self-gelling tripodna and tetrapodna.

In chapter 2, I designed composite-type hydrogel that is composed of hexapodna and gold nanoparticles for photothermal immunotherapy by expanding "self-gelling nucleic acids" technology. The AuNP-hydrogel(cg) showed strong photothermal activity and immunostimulatory activity *in vitro*. Remarkably, the hydrogel could stimulated immune cells through releasing hexapodna with its high-ordered structure that was important for CpG DNA delivery. The photothermal immunotherapy using AuNR-hydrogel(cg) presented an outstanding therapeutic effects on tumor-bearing mice. It gave thermal stress to tumor, enhanced Hsp70 mRNA expression, increased tumor associate antigen specific IgG levels, induced tumor associate antigen specific responses interferon-γ production from splenocytes to results in inhibition of tumor growth and elongation of survival. Thus, I successfully developed a novel hydrogel system for photothermal immunotherapy.

In conclusion, I successfully developed an efficient synthesis method for self-gelling polypod-like structured DNA to provide a solution to reduce synthesis cost. I also successfully developed a novel hydrogel formulation for photothermal immunotherapy by applying "self-gelling nucleic acids" technology to hybridize hexapodna and gold nanoparticles that was effective in inhibiting tumor growth.

The present investigation provides beneficial information for the further development of self-gelling nucleic acids technology based DNA hydrogel.

Acknowledgement

I have carried out these studies at Department of Biopharmaceutics and Drug Metabolism, Graduate School of Pharmaceutical Sciences, Kyoto University (京都大学大学院薬学研究科　薬学専攻　病態情報薬学分野) during Ph. D. course in 2013-2015. It would not be possible to do without the support and guidance that I received from many people.

Firstly, I would like to express my sincere gratitude and thanks to Dr. Yoshinobu Takakura, Professor of Department of Biopharmaceutics and Drug Metabolism for giving me wonderful opportunities and their support with his patience, motivation, enthusiasm, and immense knowledge. His guidance helped me in all the time of research and writing of this thesis. I cannot imagine to have a better laboratory except for his laboratory for my Ph. D. course.

I am extremely grateful to my research guides, Dr. Makiya Nishikawa, Associate Professor of Department of Biopharmaceutics and Drug Metabolism, and Dr. Yuki Takahashi, Assistant Professor. It was a great opportunity to do my doctoral program under their guidance and to learn from their research expertise. All of their encouragement, insightful comments, and hard questions are fully helpful and essential for my Ph. D. course.

I highly appreciate the supports received through the collaborative work provided from Dr. Hiroshi Sugiyama, Professor of Graduate School of Science, Kyoto University, Dr. Masayuki Endo, Associate Professor of Institute for Integrated Cell-Material Sciences, Kyoto University, and Ms. Kumi Hidaka. They kindly supported on data collection in AFM imaging in Chapter 1. I also express my sincere appreciations to the collaborative works provided from Dr. Tatsuya Murakami, Associate Professor in Institute for Integrated Cell-Material Sciences, Kyoto University, Dr. Hiroshi Imahori, Professor, and Dr. Hirotaka Nakatsuji from Graduate School of Engineering. They worked altogether with me in laser irradiation experiments, and advised me from their expertise in Chapter 2.

I would like to thank all of the students in the laboratory. They were always willing to help and give their best suggestions. Many special thanks to Tomoki Shiomi, Mengmeng Tan, Yuka Umeki, Shozo Ohtsuki for their committed support for experiments. My research would not have been possible without their assistants. I am also very grateful to all those who supported and worked together during my master course in the laboratory. Many thanks to Dr. Seiji Takemoto, Dr. Xin Guan, Atsushi Ota, Yuji Ohno, and Chika Nishizaki.

I must also acknowledge all of my colleagues in Takeda Pharmaceutical Company, Ltd. Many thanks goes to Dr. James Morley, General Manager of CMC Center, Dr. Tetsuo Hoshino, Dr. Toshio Yoshioka, Dr. Shigeo Yanai, successive Heads of Pharmaceutical Technology R&D Laboratories, Hiroshi Fukada, Masahiko Koike, Kei Mukai, Yukihiro Nomura, Yoshinobu Sato, Kazuhiro Hirata, Masahiro Niwa, Keiji Tsubota and Tetsuya Suehara.

Finally, I would like to thank all of my family. They were always supporting and encouraging me with their best wishes.

List of Publication

Efficient amplification of self-gelling polypod-like structured DNA by rolling circle amplification and enzymatic digestion.

Tomoya Yata, Yuki Takahashi, Mengmeng Tan, Kumi Hidaka, Masayuki Endo, Hiroshi Sugiyama, Yoshinobu Takakura, Makiya Nishikawa

Scientific Reports, 5,14979

Laser-responsive gold nanoparticle-DNA nanocomposite as an injectable hydrogel formulation for laser-triggered photothermal immunotherapy

Tomoya Yata, Yuki Takahashi, Tomoki Shiomi, Yuka Umeki, Shozo Ohtsuki, Mengmeng Tan, Hirotaka Nakatsuji, Tatsuya Murakami, Yoshinobu Takakura, Makiya Nishikawa

Manuscript in preparation

Inhibition of tumor growth by laser-triggered photothermal immunotherapy using polypod-like structured DNA-gold nanorod composite

Tomoya Yata, Mengmeng Tan, Hirotaka Nakatsuji, Shozo Ohtsuki, Tatsuya Murakami, Yuki Takahashi, Yoshinobu Takakura, Makiya Nishikawa

Manuscript in preparation

References

1. Dahm, R. (2005). Friedrich Miescher and the discovery of DNA. *Developmental biology*, 278(2), 274-288.
2. Pollister, A. W., & Mirsky, A. E. (1943). Terminology of nucleic acids. *Nature*, 152, 692.
3. O'Connor, C. (2008). Isolating hereditary material: Frederick Griffith, Oswald Avery, Alfred Hershey, and Martha Chase. *Nature Education*, 1(1), 105.
4. Avery, O. T., MacLeod, C. M., & McCarty, M. (1944). Studies on the chemical nature of the substance inducing transformation of pneumococcal types induction of transformation by a desoxyribonucleic acid fraction isolated from pneumococcus type III. *The Journal of experimental medicine*, 79(2), 137-158.
5. Hershey, A. D., & Chase, M. (1952). Independent functions of viral protein and nucleic acid in growth of bacteriophage. *The Journal of general physiology*, 36(1), 39-56.
6. Watson, J. D., & Crick, F. H. (1953). Molecular structure of nucleic acids. *Nature*, 171(4356), 737-738.
7. Venter, J. C. et. al. (2001). The sequence of the human genome. *Science*, 291(5507), 1304-1351.
8. Leslie, A. G. W., Arnott, S., Chandrasekaran, R., & Ratliff, R. L. (1980). Polymorphism of DNA double helices. *Journal of molecular biology*, 143(1), 49-72.
9. Crick, F. (1970). Central dogma of molecular biology. *Nature*, 227(5258), 561-563.
10. Seeman, N. C. (2007). An overview of structural DNA nanotechnology. *Molecular biotechnology*, 37(3), 246-257.
11. Seeman, N. C. (1982). Nucleic acid junctions and lattices. Journal of theoretical biology, 99(2), 237-247.
12. Rothemund, P. W. (2006). Folding DNA to create nanoscale shapes and patterns. *Nature*, 440(7082), 297-302.
13. Seeman, N. C. (2010). Nanomaterials based on DNA. *Annual review of biochemistry*, 79, 65.
14. Roh, Y. H., Ruiz, R. C., Peng, S., Lee, J. B., & Luo, D. (2011). Engineering DNA-based functional materials. *Chemical Society Reviews*, 40(12), 5730-5744.
15. Hartman, M. R., Ruiz, R. C., Hamada, S., Xu, C., Yancey, K. G., Yu, Y., Han, W. & Luo, D. (2013). Point-of-care nucleic acid detection using nanotechnology. *Nanoscale*, 5(21), 10141-10154.
16. Akira, S., Uematsu, S., & Takeuchi, O. (2006). Pathogen recognition and innate immunity. *Cell*, 124(4), 783-801.
17. Medzhitov, R. (2001). Toll-like receptors and innate immunity. *Nature Reviews Immunology*, 1(2), 135-145.

18. Kawai, T., & Akira, S. (2010). The role of pattern-recognition receptors in innate immunity: update on Toll-like receptors. *Nature immunology*, 11(5), 373-384.
19. Bianchi, M. E. (2007). DAMPs, PAMPs and alarmins: all we need to know about danger. *Journal of leukocyte biology*, 81(1), 1-5.
20. Sharma, S., & Fitzgerald, K. A. (2011). Innate immune sensing of DNA. *PLoS pathogens*, 7(4).
21. Bode, C., Zhao, G., Steinhagen, F., Kinjo, T., & Klinman, D. M. (2011). CpG DNA as a vaccine adjuvant. *Expert review of vaccines*, 10(4), 499-511.
22. Goodchild, J. (2011). Therapeutic oligonucleotides. *In Therapeutic Oligonucleotides* (pp. 1-15). Humana Press.
23. Drake, C. G., Lipson, E. J., & Brahmer, J. R. (2014). Breathing new life into immunotherapy: review of melanoma, lung and kidney cancer. *Nature reviews Clinical oncology*, 11(1), 24-37.
24. Anderson, R. P., & Jabri, B. (2013). Vaccine against autoimmune disease: antigen-specific immunotherapy. *Current opinion in immunology*, 25(3), 410-417.
25. Weiner, H. L., & Selkoe, D. J. (2002). Inflammation and therapeutic vaccination in CNS diseases. *Nature*, 420(6917), 879-884.
26. Marciani, D. J. (2003). Vaccine adjuvants: role and mechanisms of action in vaccine immunogenicity. *Drug discovery today*, 8(20), 934-943.
27. Mohri, K., Nishikawa, M., Takahashi, Y., & Takakura, Y. (2014). DNA nanotechnology-based development of delivery systems for bioactive compounds. European *Journal of Pharmaceutical Sciences*, 58, 26-33.
28. Nishikawa, M., Matono, M., Rattanakiat, S., Matsuoka, N., & Takakura, Y. (2008). Enhanced immunostimulatory activity of oligodeoxynucleotides by Y-shape formation. *Immunology*, 124(2), 247-255.
29. Matsuoka, N., Nishikawa, M., Mohri, K., Rattanakiat, S., & Takakura, Y. (2010). Structural and immunostimulatory properties of Y-shaped DNA consisting of phosphodiester and phosphorothioate oligodeoxynucleotides. *Journal of Controlled Release*, 148(3), 311-316.
30. Mohri, K., Nishikawa, M., Takahashi, N., Shiomi, T., Matsuoka, N., Ogawa, K., Endo, M., Hidaka, K., Sugiyama, H., Takahashi, Y., & Takakura, Y. (2012). Design and development of nanosized DNA assemblies in polypod-like structures as efficient vehicles for immunostimulatory CpG motifs to immune cells. *ACS nano*, 6(7), 5931-5940.
31. Sanada Y, Sakamoto S, Shiomi T, Okobira T, Mylonas E, Ohta N, Yagi N, Nishikawa M, Akiba I, Takakura Y, Sakurai K. X-ray scattering from immunostimulatory tetrapod-shaped DNAs in aqueous solution to explore their biological activity-conformation relationship. *J Phys Chem B*. 2014; 118: 10373-10379.
32. Rattanakiat, S., Nishikawa, M., Funabashi, H., Luo, D., & Takakura, Y. (2009). The assembly of a

short linear natural cytosine-phosphate-guanine DNA into dendritic structures and its effect on immunostimulatory activity. *Biomaterials*, 30(29), 5701-5706.

33. Nishikawa, M., Mizuno, Y., Mohri, K., Matsuoka, N., Rattanakiat, S., Takahashi, Y., Funabashi, H., & Takakura, Y. (2011). Biodegradable CpG DNA hydrogels for sustained delivery of doxorubicin and immunostimulatory signals in tumor-bearing mice. *Biomaterials*, 32(2), 488-494.
34. Nishikawa, M., Ogawa, K., Umeki, Y., Mohri, K., Kawasaki, Y., Watanabe, H., Takahashi, N., Kusuki, E., Takahashi, R., Takahashi, Y., & Takakura, Y. (2014). Injectable, self-gelling, biodegradable, and immunomodulatory DNA hydrogel for antigen delivery. *Journal of Controlled Release*, 180, 25-32.
35. Nishikawa, M., Takahashi, Y., & Takakura, Y. (2012). U.S. Patent Application 14/112,648.
36. Kosuri, S., & Church, G. M. (2014). Large-scale de novo DNA synthesis: technologies and applications. *Nature methods*, 11(5), 499-507.
37. Baker, M. Synthetic genomes: The next step for the synthetic genome. Nature 473, 403–408 (2011).
38. Merrifield, R. B. (1963). Solid phase peptide synthesis. I. The synthesis of a tetrapeptide. *J. Am. Chem. Soc*, 85(14), 2149-2154.
39. Lutz, J. F., Ouchi, M., Liu, D. R., & Sawamoto, M. (2013). Sequence-controlled polymers. *Science*, 341(6146), 1238149.
40. Behlke, M. A., & Devor, E. J. (2005). Chemical synthesis of oligonucleotides. *Integrated DNA Technologies*.
41. Blanco, L., & Salas, M. (1984). Characterization and purification of a phage phi 29-encoded DNA polymerase required for the initiation of replication. *Proc Natl Acad Sci*, 81(17), 5325-5329.
42. Blanco, L., Bernad, A., Lázaro, J. M., Martin, G., Garmendia, C., & Salas, M. (1989). Highly efficient DNA synthesis by the phage phi 29 DNA polymerase. Symmetrical mode of DNA replication. *Journal of Biological Chemistry*, 264(15), 8935-8940.
43. Garmendia, C., Bernad, A., Esteban, J. A., Blanco, L., & Salas, M. (1992). The bacteriophage phi 29 DNA polymerase, a proofreading enzyme. *Journal of Biological Chemistry*, 267(4), 2594-2599.
44. Reagin, M. J., Giesler, T. L., Merla, A. L., Resetar-Gerke, J. M., Kapolka, K. M., & Mamone, J. A. (2003). TempliPhi: a sequencing template preparation procedure that eliminates overnight cultures and DNA purification. *Journal of biomolecular techniques*: JBT, 14(2), 143.
45. Ducani, C., Kaul, C., Moche, M., Shih, W. M. & Högberg, B. Enzymatic production of 'monoclonal stoichiometric' single-stranded DNA oligonucleotides. *Nat. Methods* 10, 647–652 (2013).
46. Lohmann, J. S., Stougaard, M. & Koch, J. A new enzymatic route for production of long

5′-phosphorylated oligonucleotides using suicide cassettes and rolling circle DNA synthesis. *BMC Biotechnol.* 7, 49 (2007).

47. Gu, H. & Breaker, R. R. Production of single-stranded DNAs by self-cleavage of rolling-circle amplification products. *Biotechniques* 54, 337–343 (2013).
48. Lin, C., Xie, M., Chen, J. J., Liu, Y., & Yan, H. Rolling-circle amplification of a DNA nanojunction. *Angew. Chem. Int. Ed.* 45, 7537–7539 (2006).
49. AmáHong, C. & HyeáJeong, E. Self-assembled DNA nanostructures prepared by rolling circle amplification for the delivery of siRNA conjugates. *Chemical Communications*, 50(86), 13049–13051 (2014).
50. Endo, M., Katsuda, Y., Hidaka, K. & Sugiyama, H. Regulation of DNA methylation using different tensions of double strands constructed in a defined DNA nanostructure. *J. Am. Chem. Soc.* 132.5, 1592–1597 (2010).
51. Zhu, G. et al. Noncanonical Self-Assembly of Multifunctional DNA Nanoflowers for Biomedical Applications. *J. Am. Chem. Soc.* 135, 16438–16445 (2013).
52. Lee, J. B. et al. A mechanical metamaterial made from a DNA hydrogel. *Nat. Nanotechnol.* 7, 816–820 (2012).
53. Shopsowitz, K. E., Roh, Y. H., Deng, Z. J., Morton, S. W., & Hammond, P. T. (2014). RNAi-Microsponges Form through Self-Assembly of the Organic and Inorganic Products of Transcription. *Small*, 10(8), 1623-1633.
54. Zhang, Y. & Seeman, N. C. Construction of a DNA-truncated octahedron. *J. Am. Chem. Soc.*, 116(5), 1661–1669 (1994).
55. Shih, W. M., Quispe, J. D. & Joyce, G. F. A 1.7-kilobase single-stranded DNA that folds into a nanoscale octahedron. *Nature*, 427(6975), 618–621 (2004).
56. Goodman, R. P. et al. Rapid chiral assembly of rigid DNA building blocks for molecular nanofabrication. *Science*, 310(5754), 1661–1665 (2005).
57. He, Y. et al. Hierarchical self-assembly of DNA into symmetric supramolecular polyhedra. *Nature*, 452(7184), 198–201 (2008).
58. Chen, W. R., Adams, R. L., Carubelli, R., & Nordquist, R. E. (1997). Laser-photosensitizer assisted immunotherapy: a novel modality for cancer treatment. *Cancer letters*, 115(1), 25-30.
59. Li, X., Min, M., Gu, Y., Du, N., Hode, T., Nordquist, R. E., Wolf, R. F., Howard, E., Lunn, J. A., Adalsteinsson, O. & Chen, W. R. (2012). Laser immunotherapy: Concept, possible mechanism, clinical applications, and recent experimental results. *Selected Topics in Quantum Electronics, IEEE Journal of*, 18(4), 1434-1438.
60. Lepock JR. Cellular effects of hyperthermia: Relevance to the minimum dose for thermal damage. *Int J Hyperthermia* 2003;19: 252–66

61. Frey B, Weiss EM, Rubner Y, Wunderlich R, Ott OJ, Sauer R, et al. Old and new facts about hyperthermia-induced modulations of the immune system. *Int J Hyperthermia* 2012; 28:528–42.
62. Laszlo, A. (1992). The effects of hyperthermia on mammalian cell structure and function. *Cell proliferation*, 25(2), 59-87.
63. Roti Roti, J. L. (2008). Cellular responses to hyperthermia (40-46 C): Cell killing and molecular events. *Int J Hyperthermia*, 24(1), 3-15.
64. Hildebrandt, B., Wust, P., Ahlers, O., Dieing, A., Sreenivasa, G., Kerner, T., Felix, R., & Riess, H. (2002). The cellular and molecular basis of hyperthermia. *Critical reviews in oncology/hematology*, 43(1), 33-56.
65. Todryk S, Melcher AA, Hardwick N, Linardakis E, Bateman A, Colombo MP, et al. Heat shock protein 70 induced during tumor cell killing induces Th1 cytokines and targets immature dendritic cell precursors to enhance antigen uptake. *J Immunol* 1999;163: 1398–408.
66. Vabulas RM, Ahmad-Nejad P, Ghose S, Kirschning CJ, Issels RD, Wagner H. Hsp70 as endogenous stimulus of the Toll/ interleukin-1 receptor signal pathway. *J Biol Chem* 2002; 277:15107–12.
67. Asea A, Rehli M, Kabingu E, Boch JA, Bare O, Auron PE, et al. Novel signal transduction pathway utilized by extracellular Hsp70: Role of Toll-like receptor (TLR) 2 and TLR4. *J Biol Chem* 2002; 277:15028–34.
68. Noessner E, Gastpar R, Milani V, Brandl A, Hutzler PJ, Kuppner MC, et al. Tumor-derived heat shock protein 70 peptide complexes are cross-presented by human dendritic cells. *J Immunol* 2002; 169:5424–32.
69. Multhoff G, Botzler C, Jennen L, Schmidt J, Ellwart J, Issels R. Heat shock protein 72 on tumor cells: A recognition structure for natural killer cells. *J Immunol* 1997; 158:4341–50.
70. Botzler C, Li G, Issels RD, Multhoff G. Definition of extracellular localized epitopes of Hsp70 involved in an NK immune response. *Cell Stress Chaperon* 1998; 3:6–11.
71. Roigas J, Wallen ES, Loening SA, Moseley PL. Heat shock protein (Hsp72) surface expression enhances the lysis of a human renal cell carcinoma by IL-2 stimulated NK cells. *Adv Exp Med Biol* 1998; 451:225–9.
72. Multhoff G, Mizzen L, Winchester CC, Milner CM, Wenk S, Eissner G, et al. Heat shock protein 70 (Hsp70) stimulates proliferation and cytolytic activity of natural killer cells. *Exp Hematol* 1999; 27:1627–36.
73. Suzue K, Zhou X, Eisen HN, Young RA. Heat shock fusion proteins as vehicles for antigen delivery into the major histocompatibility complex class I presentation pathway. *Proc Natl Acad Sci* USA 1997;94:13146–51.

74. Suto R, Srivastava PK. A mechanism for the specific immunogenicity of heat shock protein-chaperoned peptides. *Science* 1995;269: 1585–8.
75. Binder RJ, Srivastava PK. Peptides chaperoned by heat-shock proteins are a necessary and sufficient source of antigen in the cross-priming of CD8+ T cells. *Nat Immunol* 2005;6: 593–9.
76. Zhou, F., Li, X., Naylor, M. F., Hode, T., Nordquist, R. E., Alleruzzo, L., Raker, J., Lam, S. S. K., Du, N., Shi, L., Wang, X., Chen, W. R. (2015). InCVAX–A novel strategy for treatment of late-stage, metastatic cancers through photoimmunotherapy induced tumor-specific immunity. *Cancer letters*, 359(2), 169-177.
77. Almeida, J. P. M., Figueroa, E. R., & Drezek, R. A. (2014). Gold nanoparticle mediated cancer immunotherapy. *Nanomedicine: Nanotechnology, Biology and Medicine*, 10(3), 503-514.
78. Guo, L., Yan, D. D., Yang, D., Li, Y., Wang, X., Zalewski, O., Yan, B. & Lu, W. (2014). Combinatorial photothermal and immuno cancer therapy using chitosan-coated hollow copper sulfide nanoparticles. *ACS nano*, 8(6), 5670-5681.
79. Tao, Y., Ju, E., Liu, Z., Dong, K., Ren, J., & Qu, X. (2014). Engineered, self-assembled near-infrared photothermal agents for combined tumor immunotherapy and chemo-photothermal therapy. *Biomaterials*, 35(24), 6646-6656.
80. Tao, Y., Ju, E., Ren, J., & Qu, X. (2014). Immunostimulatory oligonucleotides-loaded cationic graphene oxide with photothermally enhanced immunogenicity for photothermal/immune cancer therapy. *Biomaterials*, 35(37), 9963-9971.
81. Wang, C., Xu, L., Liang, C., Xiang, J., Peng, R., & Liu, Z. (2014). Immunological Responses Triggered by Photothermal Therapy with Carbon Nanotubes in Combination with Anti-CTLA-4 Therapy to Inhibit Cancer Metastasis. *Advanced Materials*, 26(48), 8154-8162.
82. Kumar, P., & Srivastava, R. (2015). IR 820 dye encapsulated in polycaprolactone glycol chitosan: Poloxamer blend nanoparticles for photo immunotherapy for breast cancer. *Materials Science and Engineering: C*, 57, 321-327.
83. Mirkin, C. A., Letsinger, R. L., Mucic, R. C., & Storhoff, J. J. (1996). A DNA-based method for rationally assembling nanoparticles into macroscopic materials. *Nature*, 382(6592), 607-609.
84. Giljohann, D. A., Seferos, D. S., Prigodich, A. E., Patel, P. C., & Mirkin, C. A. (2009). Gene regulation with polyvalent siRNA− nanoparticle conjugates. *J. Am. Chem. Soc*, 131(6), 2072-2073.
85. Rosi, N. L., Giljohann, D. A., Thaxton, C. S., Lytton-Jean, A. K., Han, M. S., & Mirkin, C. A. (2006). Oligonucleotide-modified gold nanoparticles for intracellular gene regulation. *Science*, 312(5776), 1027-1030.
86. Wei, M., Chen, N., Li, J., Yin, M., Liang, L., He, Y., Song, H., Fan, C. & Huang, Q. (2012). Polyvalent Immunostimulatory Nanoagents with Self-Assembled CpG Oligonucleotide-Conjugated Gold

Nanoparticles. *Angewandte Chemie International Edition*, 51(5), 1202-1206.

87. Zhang, X., Liu, B., Dave, N., Servos, M. R., & Liu, J. (2012). Instantaneous attachment of an ultrahigh density of nonthiolated DNA to gold nanoparticles and its applications. *Langmuir*, 28(49), 17053-17060.
88. Lin, A. Y., Almeida, J. P. M., Bear, A., Liu, N., Luo, L., Foster, A. E., & Drezek, R. A. (2013). Gold nanoparticle delivery of modified CpG stimulates macrophages and inhibits tumor growth for enhanced immunotherapy. *PLoS One*, 8(5), e63550.
89. Kang, H., Liu, H., Zhang, X., Yan, J., Zhu, Z., Peng, L., Yang, H., Kim, Y. & Tan, W. (2010). Photoresponsive DNA-cross-linked hydrogels for controllable release and cancer therapy. *Langmuir*, 27(1), 399-408.
90. Strong, L. E., Dahotre, S. N., & West, J. L. (2014). Hydrogel-nanoparticle composites for optically modulated cancer therapeutic delivery. *Journal of Controlled Release*, 178, 63-68.
91. Kawase, A., Kobayashi, N., Isaji, K., Nishikawa, M., & Takakura, Y. (2005). Manipulation of local disposition and gene expression characteristics of plasmid DNA following intramuscular administration by complexation with cationic macromolecule. *International journal of pharmaceutics*, 293(1), 291-301.
92. Hui Jiang, Elsa M. Materon, Maria Del Pilar Taboada Sotomayor, Juewen Liu, "Fast assembly of non-thiolated DNA on gold surface at lower pH", *Journal of Colloid and Interface Science*, 411, 92-97 (2013).
93. Chen, M. C., Huang, S. F., Lai, K. Y., & Ling, M. H. (2013). Fully embeddable chitosan microneedles as a sustained release depot for intradermal vaccination. *Biomaterials*, 34(12), 3077-3086.
94. Kono, K. (2014). Current status of cancer immunotherapy. *Journal of stem cells & regenerative medicine*, 10(1), 8.
95. Kurtz, S. L., Ravindranathan, S., & Zaharoff, D. A. (2014). Current status of autologous breast tumor cell-based vaccines. *Expert review of vaccines*, 13(12), 1439-1445.
96. Nam, J. M., Thaxton, C. S., & Mirkin, C. A. (2003). Nanoparticle-based bio-bar codes for the ultrasensitive detection of proteins. *Science*, 301(5641), 1884-1886.
97. Connor, E. E., Mwamuka, J., Gole, A., Murphy, C. J., & Wyatt, M. D. (2005). Gold nanoparticles are taken up by human cells but do not cause acute cytotoxicity. *Small*, 1(3), 325-327.